1

Ultra Micro Gas Turbines

Roberto Capata
Department of Mechanical and Aerospace Engineering, University of Roma 1, Faculty of Engineering, Roma
Italy

1. Introduction

1.1 State of art

Object of the present work is the detailed study, in every its aspect, of Ultra-Micro-Gas-Turbine Generator, that is a power device with high power density. These generators, although the covered power range oscillates between 100 and 500W, is characterized by very reduced overall dimensions: this introduces complications in the design and, above all, the realization of the mechanical components who represents the greater difficulty to exceed. The advanced searches in this field preview the realization of the characteristic structures of the machine with high tech systems:

- the impellers, both turbine and compressor, can be manufacturing with silicon, titanium or special alloys micro laser techniques (figure 1);
- the combustion chambers can be obtained in toroidal spaces with the possible lowest volume: this involves the necessity to construct fuel injection device technologically complicated, inside the same combustion chambers; a different model is constituted, in some NATO devices, by a 2-D geometry combustion chambers (an example is visible in figure 2);
- the electrical generators are constituted by a highest number of polar braces due to high rotational speed of the machine (> 100 000 rpm). Their realization is realized by micro manufacturing of planned rings that have been inserted in the case (for the statoric part), and the other ring is located on the faces the rotor impeller (usually the compressor, to avoid the high temperatures problems);
- the rotational speed is within 150 000 ÷ 350 000 rad/s (in some cases > 500.000)

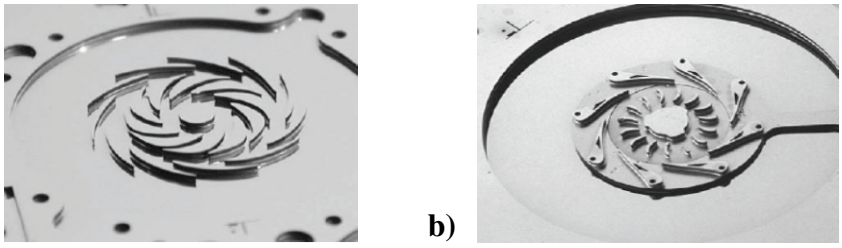

Fig. 1. Typical compressor a) and b) turbine D geometry [Epstein 2003]

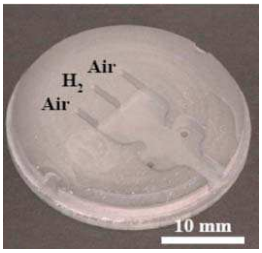

Fig. 2. Typical 2D combustor

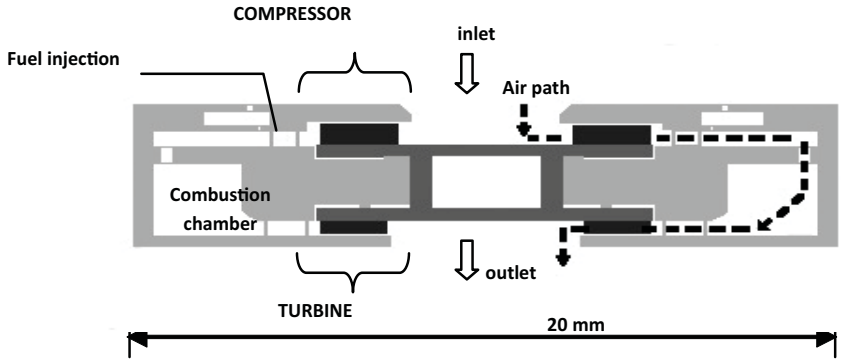

Fig. 3. MIT prototype [Epstein 1999 & 2003]

In figure 3 it shown a prototype realized from the M.I.T., that can be consider as the "symbol/emblem" of these researches carried out during the last few years in micro-turbines. It is constituted by a overlapping layers in sequence, starting from the compressor, the toroidal combustion chambers and the turbine. The characteristic data of this prototype can be reassumed in:

- Fuel: Hydrogen
- Fuel consumption: 16 g/h
- Power: 4 ÷ 10W
- Rotational speed: ≈10^6 rpm
- TIT: 1600 K
- Used materials: Si And SiC

We can notice the temperatures reached in these systems are higher than those characteristics of the actual large scale systems. Therefore, in the zones affected by the highest thermal stresses, the Silicon Si has been replaced with the most resistant SiC material. This prototype represents the highest state of the technique and the more advanced research that can be reached in this moment. Other examples of UMGT exist, however, thus do not characterized by exasperated technological levels and with a similar structure to the conventional systems. Also regarding the used materials, these device use typical steels of the commercial impellers. The thermodynamic parameters are similar to large scale sets:

- Compression ratio: ≤ 3

- Air mass flow rate: ≈ 2 g/s
- Rotational speed: ≤ 300 000 rpm
- TIT: ≈ 1300K
- Net power: 4 ÷ 100 W

2. Scaling factor

Since 90's, the academic world started to study the possibility to realize a "micro" gas turbine (GT) set, with an overall dimensions of the order of the centimetres, able to developing a nominal power within 0.10 to 100 kW. Such a type of apparatus are defined today "micro gas turbine". At the moment, the larger GT sets in service are characterized by a radial dimensions of the order of the meter and develop hundred of MW of nominal power, while the generator of a UMGT is large few millimetres, for which the elaborated mass flow rate by the micro device will be 10^{-6} times lower than a conventional machine, if the same tip speed is maintained. Moreover, the generated power will be 10^{-6} lower, consequently a micro GT device would be able, in first analysis, to producing about hundred of Watts. This value re-enters in the extremely extended field of the portable equipment applications in which the battery packages represent the main solution to the problem. The obtainable power density is greater than a conventional battery package, thanks to the fact that the power scales with the flow rate and ,therefore, with the square of the length, while the volume with the cube:

$$P \propto L^2 \tag{1}$$

$$V \propto L^3 \tag{2}$$

so:

$$P / V \propto 1 / L \tag{3}$$

Conceptually it is possible to realize any thermodynamic cycle to these scales, but it is necessary to remind that the reduced dimensions do not allow the possibility to insert any components characterized by particularly complex geometries. This consideration forces the research to adopt a simple Brayton cycle. Other considerations concern the fluid dynamical behaviour of the device and the mechanics of the machine, which will modify the relative choices to the thermodynamic cycle, moving the optimal design parameters in different zones from those developed for a classic large scale machine. In fact, while the speed and the temperatures are almost unchanged regarding the macro turbines, the chord blade is of the order of millimetre. The consequence is that the value of Re number is lower than the actual conventional large scale turbo machines (usually between 10^5 - 10^6). Viscous forces will have greater influence and the relative losses will be more evident. The losses linked to the three-dimensional aspect of the device, to the clearance between case and disc or to shock waves will be more significant and higher than the common ones. It is reasonable to think that the increase of the viscous forces produces higher losses for aerodynamic resistance in the piping and/or manifolds. One of the problems that the research/designer must be faced in the study of the micro fluid dynamic phenomena is the adequacy of the continuous fluid model. To evaluate the possibility of adopting the Navier-Stokes equations, the Knudsen number Kn, equal to the ratio between the free medium path of particles and

characteristic length, can be used. Several tests have evidence that the first effects of the non-continuity appear for values of Kn = 0,1, while the continuous model loses its validity to Kn = 0.3. Considering that the free medium path of the air, at atmospheric conditions, is 70 nm (nanometres), the flow will have to be considered discontinuous for lengths of 0.2 μm. The considered micro devices dimensions (the gap will be of the order of some μm) the flow can be still studied as continuous, therefore it is not necessary to consider the molecular kinetic. The heat exchange between the device components and with the fluid is higher, due to the small scales of length, for which the thermal gradient will be lower and consequently thermo-mechanical stress will be lower. On the other hand, the parts isolation will be more complex and the heat losses towards the outside will be higher. The materials deserve a detail attention since the reduced scales allow the introduction of light ceramic material, with very attractive mechanical properties, but - to large-scale -unusable for the GT construction. With these dimensions, in fact, the material can be still considered as a continuous one, for which the plastic, the elastic, the creep and the oxidation behaviour, and finally the coefficient of thermal conduction, do not change, while the mechanical resistance is greater, strongly dependent on the manufacturing defects that are "naturally" limited by the micro-dimensions.

3. Thermodynamic cycle

Generally, the thermodynamic analysis of a system is independent by the scaling factors; theoretically it is possible to adopt any type of cycle to the micro-scales without particular attention. The technological limits, the inherent mechanical and fluid dynamical considerations and the necessity of device compactness, impose limited and important choices. In the case of the UMGT, it has been decided to privilege, fundamentally, the compactness and simple manufacturing, to contain the costs, admitting not optimal machine efficiency. This choice does not involve any particular disadvantages, since from theoretical extrapolations show sufficient efficiencies, to obtain higher energy density than to the best actual battery packages. The thermodynamic cycle adopted, in terms of simplicity, is the Brayton cycle, that has moreover the advantage to supply increasing energy density with the increase of the operational speed. The main disadvantage is the necessity in such case to have a component efficiency at least to the 40-50% for being self-sustainable: it must, therefore, be headed at most efficient and possible productive technologies. The state of the art for thus small structures renders the integration of conventional cooled or regenerated cycles improbable, but remains the possibility to use the outlet fluid of the compressor to cool the walls of the combustion chamber, or to obtain a sort of pre-heating, without to complicate geometry. To obtain a thermodynamic cycle adapt to the prefixed scope, the outlet temperatures of the combustion chamber must be comprised between 1200-1600 K and the tip speed between 300-600 m/s, consequently stresses will be of the 10^2 order of MPa for compression ratios between 2:1 and 4:1. Wanting, at least, to privilege compactness and lightness the choice of radial machine is most suitable, thanks the possibility to use a single stage for compressor and turbine. The influence of the Reynolds number on the performance of turbo machines has received considerable attention in literature, and several more or less general and sufficiently reliable models have been demonstrated, both for incompressible and compressible flows. Historically, the first formulations originated from empirical data collected on hydraulic turbine models and yielded acceptable results for full-scale applications. It is clear that the scaling for other types of machinery -and specifically

for radial pumps and compressors- was much more sensitive to additional factors, e.g. the different relative roughness of the full-scale machine with respect to the model, leakage effects due to the geometric non-similarity of machining tolerances and clearances, and both the lack of data and the excessive measurements uncertainty in the smallest models. There have been numerous attempts to formulate a general model of $\eta = f(Re)$ scaling, but all the proposed models agree with the experimental data only within a limited range of configurations and fall therefore short of representing general design correlations. The main problem of the available formulations seems to be on the one side their complexity and on the other side the non-crisp phenomenological model they subsume, but the common point in all approaches is the distinction in Reynolds dependent and independent efficiency losses. This assumption leads to unavoidable difficulties in the determination of the Re-independent loss fraction, mostly originated by non-homogeneous factors like manufacturing methods, tolerances and clearances. An interesting series of experimentally validated studies were conducted in the 80's for single and multistage centrifugal compressors by Wiesner [Wiesner 1979], Casey and Strub: the results of these investigations differ from Author to Author, as do their respective conclusions, but one common point all agreed upon is the definition of a reference Reynolds number based on the width of the exit section:

$$\mathrm{Re} = \frac{U_2 b_2}{\nu} \tag{4}$$

By contrast, since we are interested here in introducing correction factors to the Balje charts, it was necessary to adopt the same choice of parameters: therefore, in this work the *Re* definition as reported in [Balje 1981] has been used throughout:

$$\mathrm{Re} = \frac{U_2 D_2}{\nu} \tag{5}$$

Some scaling formulations include the influence of Reynolds number and surface roughness, but in this work we consider only hydraulically smooth surfaces, eliminating thus the roughness variable from the picture, also in consideration of the rather scant data available on the few prototypal rotors in the ultra-micro scale range. The derivation of a "universal" formula is intrinsically difficult, due to the substantial difference in the flow phenomenology, so that each class of machines requires a specific analysis. The objective of this work is to propose a preliminary method to scale the efficiency of ultra-micro-compressors and turbines, investigating the possibility to extend the applicability of Balje charts for miniaturized machines, to reduce design time- and resources investment.

3.1 Reynolds number effects – Problem formulation and coefficient definition

The general functional relationship proposed in the available references is of the so-called Stodola form:

$$\frac{1-\eta}{1-\eta_{\mathrm{ref}}} = a + (1-a)\left[\frac{\mathrm{Re}_{\mathrm{ref}}}{\mathrm{Re}}\right]^n \tag{6}$$

Whereas the coefficients *a* and *n* differ from Author to Author, as represented in Table 1.

Year	*Source*	*Inviscid loss fraction"a"*	*Viscosity-dependent loss fraction (1-a)*	*Exponent n*	*Machine type*
1925	Moody	0.25	0.75	0.33	Propeller turbines
1930	Ackeret & Muhlemann	0.50	0.50	0.20	Hydraulic turbines
1942	Moody	0.00	1.00	0.20	Pumps
1947	Pfleiderer	0.00	1.00	0.10	Pumps
1951	Davis, Kottas & Moody	0.00	1.00	variable	All turbomachines
1954	Hutton	0.30	0.70	0.20	Kaplan turbines
1958	Rotzoll	0.00	1.00	variable	Pumps
1960	Wiesner	0.50	0.50	0.10	Radial compressors
	Fauconnet	0.24	0.76	0.20	
1961	O'Neil & Wickli	0.00	1.00	variable	Radial compressors
1965	ASME Code PTC-10	0.00	1.00	0.20	Axial compressors
		0.00	1.00	0.10	Radial compressors
1971	Mashimo et Al.	0.25 min	0.75 max	0.20	Radial compressors
1974	Mashimo et Al.	0.15-0.57	0.43-0.85	0.20-0.50	Radial compressors
2007	Capata, Sciubba & Silva	0.50	0.50	0.25	All turbomachines

Table 1. Summary of the most popular efficiency correction equations

Where the coefficient *a* represents the Reynolds number independent loss fraction, but it is in fact sometimes itself a function of *Re*, and the exponent *n*, as proposed in Strub [Strub 1987], is in general taken to be inversely proportional to the Reynolds number: this approach accounts for the decreasing influence of the viscous losses for high values of *Re*. The main shortcomings of this approach are:

- The coefficient *a* is likely to remain constant only in a small range of Reynolds numbers;
- The Re-independent losses are also related to other factors like for example leakage;
- It is also well known that *a* varies with both geometry and manufacturing techniques even for machines with the same *Re*. As a first approximation, we assumed that the manufacturing process and clearances fit with the parameters imposed for the Balje charts. This assumption is not far from reality, because the design of such small devices is strongly constrained by factors unrelated with fluid-dynamics, so that ultra-micro-machines are indeed all quite similar to each other, and because the estimated clearances [Epstein 2003] are in the same range as those reported on the Balje charts.
- The exponent *n* varies considerably from author to author and this might depend on the different intrinsic accuracy of the data used by different authors, originated by the neglection of the effects of relative roughness. As stated above, in this work we concentrate on the influence of the Reynolds number, thus as a first step we, too, neglected the relative roughness, especially because we could find no experimental data in the range of the geometrical scales of importance here. Wiesner [Turton 1984] pointed out that it is useful to introduce an explicit Re-dependence in this exponent, and proposed a functional relation of the form:

$$n = k' \left(\frac{1}{Re/Re_{ref}} \right)^{k} \tag{7}$$

Notice that Equations (6) and (7) appear to be "complex" enough (i.e., to subsume a deep enough phenomenological model) to yield a good estimate of the losses for a particular class of machines such as the ultra-micro ones considered here. To circumvent the lack of a large experimental database, we decided to follow a different "type" of empirical experiments, in which numerical simulations substitute for laboratory tests. A sufficiently large set of data was created by means of accurate numerical simulations, and values for the constants a, k and k' in equations 6 and 7 above were obtained by a best fit procedure. Thus [Capata & Sciubba 2007] the final formula we propose for the scale-down is:

$$\frac{1-\eta}{1-\eta_{\text{ref}}} = 0.50 + 0.50 \cdot \left[\frac{\text{Re}_{\text{ref}}}{\text{Re}}\right]^{\left[0.084 \cdot \left(\frac{\text{Re}_{\text{ref}}}{\text{Re}}\right)^{0.25}\right]} \tag{8}$$

The coefficients in equation (8) provide a good agreement with the values reported in literature, particularly with the model by Wiesner. An direct confirmation of the validity of our procedure was obtained by applying equation (8) to compute the efficiency of an ultra-micro compressor designed by the research group at MIT. Finally we suggest to adopt a polytropic efficiency within 0.55 and 0.7 in the preliminary design of the turbomachines.

3.2 The thermodynamic CYCLE – General overview

The cycle equation sets are:

$$p_2 = p_1 \beta_c \tag{9}$$

$$T_2 = T_1 \beta_c^{\frac{k_c - 1}{k_c \eta_p}} \tag{10}$$

$$T_4 = T_3 \left(\frac{1}{\beta_t}\right)^{\frac{(k_t - 1)}{k_t} \eta_p} \tag{11}$$

where p_1 is the inlet static pressure equal to 1 atm, p_2 is the compressor outlet static pressure, T_1 and T_2 the temperatures of beginning and end compression process respectively, and T_3, T_4 refer to the turbine expansion. The compression ratio $\beta_c = 2$ is different from the expansion ratio $\beta_t = 1.94$, due to the combustor losses (approximately 3%). Once that the static temperatures in the main points of the cycle are known, it is possible to evaluate the mixture ratio α and the equivalent ratioϕ. Then, the compression work W_c the expansion one W_t and combustion process Q, can be calculated:

$$W_c = \int_{T_1}^{T_2} c_{p_{air}} dT \tag{12}$$

$$W_t = \int_{T_3}^{T_4} c_{p_{mix}} dT \tag{13}$$

$$Q = \int_{T_2}^{T_3} c_{p_{mix}} dT \tag{14}$$

remembering that the molar fractions (necessary to calculate the $c_{P_{mix}}$) are obtained from the equivalence ratio:

$$\frac{n_{C_nH_m}}{n_{air}} = \phi \left(\frac{n_{C_nH_m}}{n_{air}} \right)_{stech} \tag{15}$$

$$x_{C_nH_n} = \frac{n_{C_nH_m}}{n_{C_nH_m} + n_{air}} \tag{16}$$

$$x_{air} = 1 - x_{C_nH_m} \tag{17}$$

Once defined the net work W_u, it is possible to determine the actual thermodynamic efficiency η_{th}:

$$\eta_{th} = \frac{W_u}{Q} \tag{18}$$

The net power can be calculated as follows:

$$P = \eta_e \dot{m}_{air} \left[\left(1 + \frac{1}{\alpha} \right) \eta_m L_t - \frac{L_c}{\eta_m} \right] \tag{19}$$

$$\dot{m}_{C_nH_m} = \frac{\dot{m}_{air}}{\alpha} \tag{20}$$

And the global efficiency η_g is:

$$\eta_g = \frac{P}{LHV \cdot \dot{m}_{fuel}} \tag{21}$$

4. UMGT component analysis

The first goal in the design of an UMGT is to contain the device overall dimensions and to avoid, if possible, a multi stage configuration: wanting to obtain a reasonable compression ratios, the choice falls on radial machine (centrifugal compressor and centripetal turbine). Being the thermodynamics invariant regarding the macro turbines, to generate the required specific power with single stage machines, it will be, however, necessary to adopt compression ratios between 2:1 and 4:1 and TIT within 1200 - 1600 K. Higher temperatures has to be avoided, due to the difficulty to integrate a cooling system. The centrifugal stresses (most important), as the specific work, depends on the square of the speed, that implies for, the considered values of U (velocity), between 300 and 600 m/s, stresses in the order of the hundreds of MPa. Not being able to take advantage of the conventional turbomachines manufacturing techniques and considering the various fluid dynamic problematic at the micro scales, it will be necessary to study which parameters of the conventional design are still adaptable and, where is necessary to act ex-novo in order to redefine an optimal area of design. The most important constrain in the design procedure is the adoption of 2-D extruded geometries for the blades, using the photolithography techniques, now widely diffuse for the production of MEMS (Micro Electro-Mechanical-Systems). Fortunately

continues steps in the development of such manufacturing techniques has been recognized and more complex 3-D geometries can be, nowadays, produced. An other design constraints are the maximum obtainable blades heights. This value, with the laser techniques, was limited to 500 μm few years ago, but now it is possible to obtain higher values, clearly, with greater costs. The Reynolds number is lower than conventional machines and considering the several constructive limits, will be difficult to succeed to create a geometry to avoiding separation, moreover the net output power will be probably lower than the hypothetical one with simple scale considerations. The work will be, substantially, produced by the mass forces. The conventional radial machines, usually, are equipped with inducer or exducer and, guided through sweet bending of the channels through the rotor, in such way to guarantee the lower possible losses for the interaction between boundary layer and angles or the flow separation: in this case it could not be constructively simple or favourable economically to realize a rounded inlet manifold or an axial outlet channel. Considering the diffusive process of the compressor, it could be useful to increase the chord length and to compensate the absence of constriction in the channel, increasing the blade thickness, in particular the trailing edge will be thicker than conventional machine. Consequently, the more opportune choice could be the reduction of the gap between the rotor and the case, to decrease the ventilation losses, but to minimize such distance implies to increase the resistance losses for the low blade height. Recent studies of the MIT have evidenced that a good strategy to such scale is to realize a gap equal approximately to 1% of the blade height. The problem of the flow separation in turbine is less problematic than in the compressor. The Reynolds number value is about 10^4 or lower, due to the elevated temperatures produced by the combustion. The significant losses will be at the flow exit, due to the straight angle (90°) and of the swirl residual. To partially recover this residual a diffuser will be insert.

4.1 Combustion chamber at MIT

Undoubtedly, the combustion chamber plays a crucial role in the design of the entire device, considering, above all, the necessity to limit the dimensions. The main requirements of a combustor are high efficiency, low pressure drops, high structural resistance and low emissions. Surely, for a conventional combustor is simpler to obtain these requirements, thanks to the ability to realize - to the macro scales - complex structures. In favour of a micro combustor there is an higher energy density, coupled to a greater elaborated flow rate for volume unit, as can be noticed in table 2.

In a UMGT, the relative volume, will be, approximately, 40 times greater than a traditional system. The largeness of the combustion chamber, in fact, is dictated by the necessity to completely develop the reactions and by the residence time, that it is the sum of the necessary time to the mixing (that scales with the dimensions of the device) and the chemical reaction time (that is fixed and forces to consider greater volumes at the micro scales). In a conventional engine, beyond 90% of the residence time is reserved to the mixing. At this point it is useful to introduce the number of Damkohler "Da", that it is the ratio between the fluid dynamic time, (how much time the fluid spends to cross the combustion chamber) and the chemical reaction time. Experimentally it is verified that, for having a complete reaction, it is necessary to have Da number higher the one (Da > 1). In a combustor is fundamental to obtain the highest possible energy density, and to achieve this objective, is necessary to be capable to maintain high flow rate for volume unit. Moreover is necessary to avoid to increase the chamber dimensions. At the same time it is fundamental

	Conventional Combustor	Micro combustor
Length	0.2 m	0.001 m
Volume	0.073 m^3	6.6 10^{-8} m^3
Cross-sectional area	0.36 m^2	6 10^{-5} m^2
Inlet total pressure	37.5 atm	4 atm
Inlet total temperature	870 K	500 K
Mass flow rate	140 kg/s	1.8 10^{-4} kg/s
Residence time	7 ms	5 ms
Efficiency	> 99%	> 0.9
Pressure ratio	> 0.95	> 0.95
Exit temperature	1800 K	1600 K
Power density	1960 MW/m^3	3000 MW/m^3

(note: the residence times are calculated using inlet pressure and an average flow temperature of 1000 K)

Table 2. Comparison between a conventional combustor and a micro combustor [MIT prototype – Epstein 2003]

to maintain the Damkohler number higher than the unit. It can act in two ways: increase the fluid dynamic time to complete the combustion or decrease the necessary residence times. Clearly, the first choice contrasts with requirement of maximum energy density, since previews the greater dimensions, while, the second one, is applicable with good result by the use of catalysts. The greater surface/volume ratio of a micro combustor increases the efficiency of catalysts, accelerating the chemical reactions. In this case the heat losses are not negligible, as well as in the traditional systems, since an overall efficiency and reaction temperature reduction have been produced. In effects it has been demonstrated that the relationship between lost heat and generated heat is inversely proportional to the inverse of the hydraulic diameter of the combustion chamber:

$$\frac{Q_{lost}}{Q_{prod}} \propto \frac{1}{D_{hyd}^{1.2}} \tag{22}$$

The hydraulic diameter of a micro combustor is of the order of millimetre, one hundred times lower than conventional one. This fact implies that the heat losses correlated to the heat produced by the combustion will be approximately one hundred times higher than the traditional combustors. For these reasons will be improbable to achieve an efficiency of 99% compared to the commercial systems. Finally, a reaction temperature drop increases the reaction time. All these factors reduce the available "design space", as consequence of an important decrease of the Damkohler number, and the flammability range, due to the reaction time decrease. Clearly the choice of fuel completely modifies the design limits and, maybe, the conditions will be more restrictive. An effective way to reduce the residence times is the insertion of a premixing device, for example immediately after the compressor exit, after the "flame holder", so that the mixture reaches the combustor very stirred: this can produce backfire problems and instability, but the residence time is reduced of a factor 10 regarding conventional 5-10 ms. A method to reduce the heat losses and, at the same time, to cool the combustor walls consists in leading the compressor outlet air around to the external wall of the chamber. This technique derived directly from the conventional inverse flow combustor, the only difference is that the liner is cooled for conduction rather than through a fluid film. The configuration with premixing device previews the fuel injection before the chamber inlet, to begin the mixing with the air and to reduce the dimensions of

the device. The relative technologies to the photolithography are extremely favourable for the injectors manufacturing. The choice of the materials represents an other design crucial point; the silicon introduces serious problems of plastic deformation at 950 K. A combustor with a dilution zone (for cooling the flow) can be adopted, and materials like silicon carbide SiC presents an higher thermal resistances. Remember that the thermal fluxes, previously discussed, facilitate the walls cooling. The dilution ("Dual zones") extends the range of the elaborated flow rate, but at the same time decreases the obtainable maximum efficiency of 10-20%. These combustors have been tested with an outlet temperatures of 1800 K approximately.

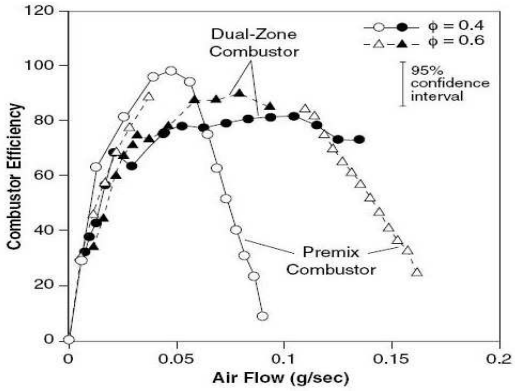

Fig. 4. Combustion efficiency of an hydrogen micro combustor [Peirs 2003, Epstein 1997, 2003]

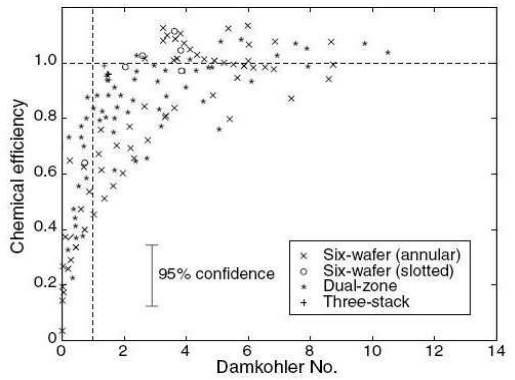

Fig. 5. Combustion efficiency to varying the Damkohler number

The necessity to assure the flame stability introduces more difficulties, so the configuration with dilution zone facilitates the recirculation in the primary zone through the air that enters in the secondary zone. Moreover the mixture ratio (in this case close to the steichiometric one) allows to decrease the reaction times. The adoption of the slots increases the turbulent phenomena in the chamber. Other fuel (as ethylene, propane, butane, methane, ecc) and other configurations (with platinum catalysts) have been tested and all the data are collected in Figure 5 figure according to the Damkohler number. It is evidenced how it is necessary to work with Damkohler numbers at least equal to 2, to obtain good combustion efficiency.

4.2 Other combustion chamber

Here follow is reported a particular case of a built and tested ultra micro combustion chamber.

4.2.1 UDR1 UMGT combustion chamber

The 2.5 kW UDR1 UMTG is composed of a compressor, a compact air pre-heater (the pressurized air exiting from the compressor is heated by ΔT= 393 K), a combustion chamber and a turbine, that together compose the thermal section; a double effect (reversible) electrical engine for the electric part; a shaft and the bearings for the mechanical, and obviously all the auxiliaries components required, as valves, controllers, and ducts, including the management unit. For safety reasons the cylindrical fuel tanks are external to the metallic UMTG enclosure [Capata & Sciubba, 2010].

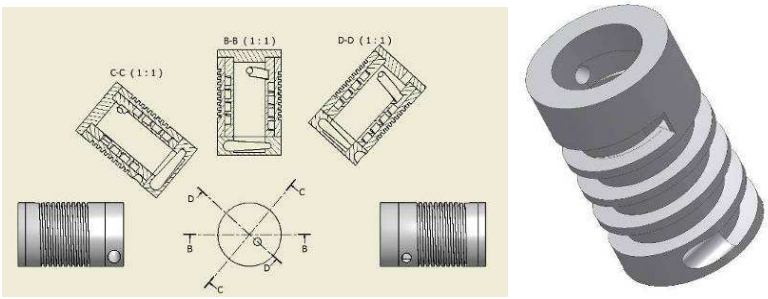

Fig. 6. CAD rendering of the combustor with a detailed view of the pre-heater.

The overall length of the assembled and modified combustion chamber is 2.2 cm, the outer diameter 4.2 cm and the overall height is 13.0 cm.

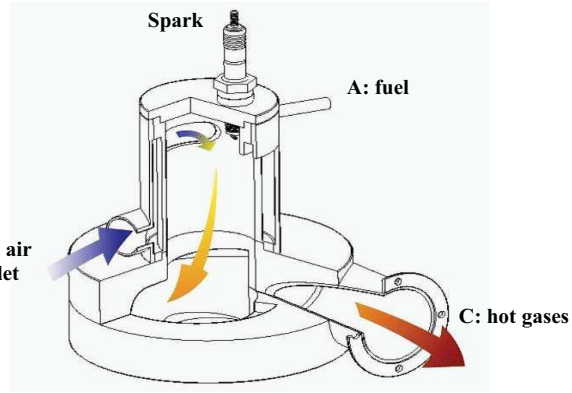

Fig. 7. The tested prototype of the combustion chamber

4.3 Bearings and rotor dynamics

A UMGT is characterized by highest angular velocities (1 or 2 orders of magnitude higher than conventional ones) and by clearance between the components of the order of the

micron. It is therefore from is easy to verify as the great part of the design development is dedicated to the bearings and to the rotor dynamics. The first reflection is, due to the high rotational speed (> 20000 rad/s), the device will work in supercritical conditions, with operational frequencies higher than the resonance ones and for this reason the study of the stability will be primary in the machine design. Clearly the bearings play a dominant role in the rotor dynamics as they must support axial and radial thrust of the rotor, dampen the oscillations and support the forces deriving by the accelerations of the rotary parts, without to count the electric forces and the operational pressures. It cannot certainly be neglected that the supports must be able to supporting the high turbine temperatures and the thermal gradient presents and, then, be able to work in any operational condition. At last the resolution of all these problems must be consider the actual technological limitations. Other devices MEMS with rotary parts currently exist, but the angular velocities are such to allow to using not-lubricated bearings. Moreover do not exist in commerce such "little bearings" to be used for these rotors. Honestly, we have to mentioned two manufacturers that guarantee dry bearings at 200000 rpm (20933 rad/s). Therefore, the academic study focuses on two possible solutions: electromagnetic or air bearings. The first solution introduces the possibility to take advantage of magnetic fields or electrical ones to support the rotors loads. The problem relatively to the magnetic fields resides in the impossibility to adopt ferromagnetic materials in the productive technologies chosen (recording laser and photolithography), moreover the Curie point is such configuration not to allow of using these systems to the temperatures previewed in turbine and would be therefore necessary to introduce a cooling system, with all the design constraints and possibilities connected. Studies have been carried on the electric fields, but the forces that are succeeded to produce are decidedly inferior to support the considered loads. To all these consideration we must add that the electromagnetic bearings are strongly unstable and required a feedback control systems, which would complicate the installation. The air bearings introduce numerous advantages, in particular in terms of constructive simplicity, of loads capability, and relative insensibility to the problem of the high temperatures. Currently these device are already used for medium-small dimensions turbomachines. At smaller scales the gas bearings are wide used in micro gyroscopic system since many years. Wanting to make scale considerations it can be said that, to parity of load conditions, the ability of these bearings grows up with the overall dimensions decrease, because the ratio volume/surface decreases and consequently the inertial load. Certainly the rotor dynamics results to be, partially, simpler (the introduced structure is more rigid, if compared to the conventional ones), thus allowing the approximation of the rigid body. The development of the bearings has to preview two different use: first, the bearings must support the radial loads, second, must support the axial loads. These bearings are composed from a cylindrical hinge in contact with a lubricating support. More efficient models exist, but considering the complexity of the system, the more reasonable choice is the first one. The lubricating fluid in our case is air in pressure and according to how it is injected, the bearings are distinguished in "hydro-static" if the source is external and "hydrodynamic" if the support forces are directly generated by the spin of the disc (figure 8). Mixed configurations are possible (figure 9). Since the UMGT includes a compressor is possible to adopt both the configurations, and both solution are able to satisfying the loads requirements and temperatures stresses to these dimensions. The two types of bearings are characterized by various dynamic characteristics. In the hydrodynamic bearings the load ability grows up to increasing of the rotational speed, because the pressure of the film between disc and support increases with the spin. In theory, also for a hydrostatic bearing a mechanism of this type can be fed; we

can imagine to support the gas in pressure through the compressor which will consequently regulate the pressure of the lubricating fluid. If the pressure of the fluid were maintained to constant the load ability would decrease gradually to increasing of the speed. In figure 10 is visible a comparison between the two types of bearings and a conventional one. In an hydrostatic bearings, pressure is maintained constant, while for an hydro dynamic one the load capability cargo depends on the speed and L/D ratio, where L is the length of the bearing while D is the diameter of the rotor. To decrease of this ratio the performances gets worse.

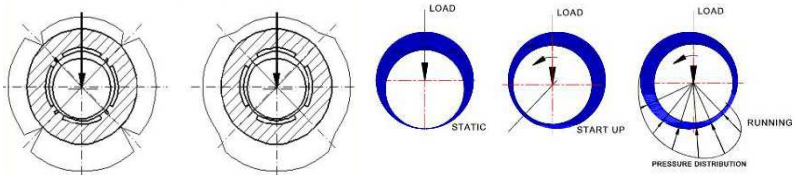

Fig. 8. Operational mode of a hydrostatic bearing (over) and hydrodynamic (under)

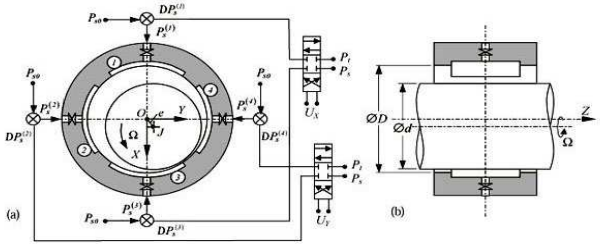

Fig. 9. Hybrid configuration

The fluid simply "sprayed" outside by the considered load, rather than to develop an adequate profile of pressures to balancing the external force. Unfortunately, in the laser manufacturing exist technological constraints, that does not allow to obtain elevated L/D ratio. Other parameters that influence the bearings design are the ratio between gap and the length of the bearing g/L, the mass of the rotor, the Reynolds number; while for the hydrodynamics bearings the load capability is dominated by the inverse of $(g/D)^5$ ratio. Currently the DRIE techniques allow to realize aspect ratio of 30:1, but a value of 100:1 can be reached. This means that assuming gap of 10-20 μm (that is the minimum value can be adopted to avoid the rotor failure for contact) can be had lengths of the channel of lubrication of 300-1000 μm. The design of an hydrodynamics bearing would suggest to us to decrease the g/D ratio and, therefore, to choose rotors with possible greater diameter, but this contrasts with the requirement of maximizing relationship L/D. Such parameters will probably find outside the normal design range. As already said the rotor operational frequencies are much higher than the resonance ones, and to such frequencies it is possible to model the bearing as a complex of springs and dampers whose effect is given by the lubricating gas which is cause also of operational instability due to transverse forces. The gap it must be such to support a deviation of the rotor during the "crossing" of the critical frequencies without to hit the support. Figure 11 shows the MIT data (rotor diameter of 4 millimetre and gap of 12 μm). It can be noticed as the maximum displacement is lower than the maximum allowed. The data is in agreement with a famous analytical model, known as

"Jeffcott wheel": to low frequencies the rotor rotate around the geometric centre, while to at high frequencies rotates around the centre of mass. The dotted line represents just the loss of balance between geometric centre and centre of mass to which asymptotically stretches the rotor. For a hydrostatic bearing the critical frequency scale, simply, with the pressure and the viscous damping decreases to increasing of the speed. The amplitude of displacement of the rotor to the critical frequencies, then, increases with increasing of the pressure.

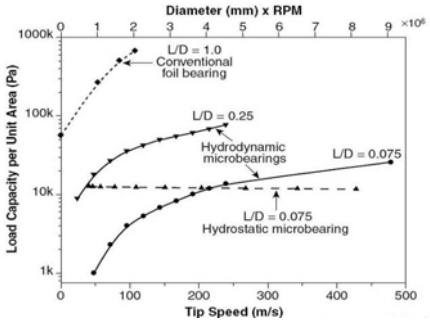

Fig. 10. Comparison between the load abilities of several bearings [Van den Braembussche 1993]

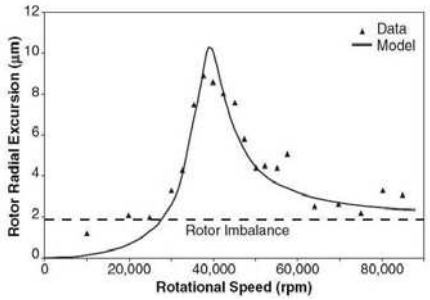

Fig. 11. Behaviour of an air micro bearing [Epstein 1997]

The trend will be similar to that reported in Figure 12, but to increasing of the pressure the peak will be moved up towards right and, this suggests to cross the critical frequency at low pressure values and low speed to, then, increase the pressure and to harden the bearing. A factor that influences the relative displacement amplitude at the critical frequency and the instability phenomena is the balance loss of the rotor. Normally the conventional machines adopt a dynamic balance that substantially consists in measuring the loss of balance and to modify the mass locally, to compensate the displacement between geometric centre and centre of mass. In the micro machines such problem is less sensible (the loss of balance for a rotor of 4 millimetre is about 1-5 μm) because the manufacturing process uses Si mono crystals or wafer of material much homogenous. To this can be add the manufacturing precision of ~1 μm. That it renders geometry much uniform. On the other hand must pay great attention to the alignment of the wafer. The hydrostatic bearings have the advantage of being stable to all the speeds within a fixed range, on the contrary the hydrodynamics ones suffer to low speed, while they are perfectly stable to the high ones. A way to stabilize these last bearings is to apply a unidirectional force that presses and pushes the rotor

towards the wall of the support and, conventionally, the weight of the disc is used to generate such forces. The common method to quantify the decentralization necessary to create such forces is given by the eccentricity, ratio between the distance wall-rotor on medium gap (the 0 if the rotor is cantered, 1 if it touches the wall). The problem to the micro scales is that inertia is practically uninfluenced regarding the surface forces, this is favourable if we consider that the device demands orientation independence, but in terms of stability it has pushed to find such lay outs that take advantage of a heterogeneous distribution of the gas pressure to generate eccentricity. The zone behind the rotor is subdivided in two rooms that can be pressurized independently. Such system has been largely simulated and the result show that the rotor is stable for eccentricity values over 0.8-0.9. A "not yet solved" problem is related to the axial flows that pass in the interstice between rotor and support of the bearing: considering dimensions of the gap these flows do not seem negligible neither in hydrodynamic neither in that hydrostatic one. The stability, as we said, strongly depends on the $(g/D)^5$ ratio through a mass parameter:

$$\bar{M} = \frac{mp}{72L\mu^2}\left(\frac{g}{D}\right)^5 \tag{23}$$

It can be noticed that is necessary to have high eccentricities to having a gap, locally, more little. In this manner mass parameters decrease and, as consequence, the dotted line in figure 12 will be lower. The conventional turbomachinery succeed to obtain a minimal eccentricities closed to 0.5, but to our scales we are limited in the choice of the shape ratio.

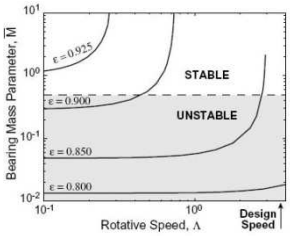

Fig. 12. Gas bearing stability in function of the eccentricity and normalized rotational speed [Freccette 2003]

Thus high eccentricities imply high accuracy in the circularity of the rotor parts and support, with the maximum shunting lines in the order of the μm, to avoid interferences. To adopt high eccentricities can be problematic in operating terms, because they produce a strong balancing losses. To obtain better performances could be the adoption of so-called "wave" bearings. This device is capable to dampening the whirl effects due to the excitation of the pressure perturbations generated by the particular geometry of the same bearings. This advantage does not involve some constructive complication and can be easy implemented through the photolithography techniques, however since the technological constraints define a minimal gap, the only way to create such geometry are to increase the interstices. From a performances analysis results that the load capability decreases, but the stability strongly increases and the minimal demanded load to stability operate (that means the minimal value to obtain the minimal stable eccentricity) decreases. Being the load capability of the bearings more sufficient than the required one, its decrease, in favour of the stability,

would not be problematic for the correct operational mode of the device. Regarding the thrust bearings necessary to support axial stresses, both the hydrostatic configuration than the hydrodynamic one has been successfully tested and verified. In both cases the working point is sub critical, that is the exercise frequencies are under the critical ones, and this bring to an important design simplification. The hydrostatic bearings have a stationary behaviour and lead pressurized air in contact with the rotor through orifices circularly located inside the support. A value of about 2-5 atm (0.2÷0.5 MPa) are necessary to obtain adequate load capabilities and a good rigidity. The maximum rigidity is obtained when the pressure drop through the orifices equals the radial flow from the drainage edge of the bearing. The hydrodynamic bearings take advantage of the viscous resistance, exalted from a superficial envelope of spirals, to generate of the pressure gradient on the surface that increases towards the centre of the rotor. This mechanism self sustains and does not demand constructive complications, reducing the number of wafer necessary too. It is considered, moreover, that, while at the conventional scales, this type of bearings are less effective and not so used, at the small scales, thanks to the great increase of the superficial forces, regarding the volumetric ones, the load capability and the rigidity are similar to the ones of the high speeds hydrostatic bearings. This system introduces a problem of the minimal speed to generating a sufficient pressure to eliminate the rotor rubbing with the static parts: fortunately such minimal speed is of the order of 10^4 rpm [Epstein, Jacobson, Spakovszky] and this implies a malfunctioning limited to machine start up. The power dissipation of the two types of bearing has been calculated and verified by MIT institute and appears to be low. The necessity to obtain high accuracy in the bearings manufacturing, is in contrast with the demand of a device series production with an only one wafer. The plasma techniques, as well as all manufacturing techniques, introduce heterogeneous problems, that increase moving from the centre towards the periphery of the wafer. Regarding DRIE process, that is still in phase of maturation, seems that the manufacturing process carry to an inaccuracy in the recording depth of 3 μm on a diameter of 4 millimetre for the peripheral devices (the most penalized), than consist in a rotor loss of balance and, therefore, a total malfunctioning of the bearings. Actually MIT reports to have been tested this kind of bearings at a rotational speed of about 1.4 Mrpm [Epstein 2003]

4.4 Auxiliaries

The most important efforts in the UMGT design are dedicated, undoubtedly, to the turbomachines, the combustion chamber and the bearings. But we have to consider that the others components that completing the device will not be simpler designed or less important, being the system, in its entirety, a good compromise between the several parts, a compromise between the obtainable good characteristics from every single piece.

4.4.1 Electric generator and starter

The literature on the electric motors is extremely huge, but on the micro generators is insufficient. Seen the high temperature operational conditions, the necessity to integrate the components to avoid ulterior complications dictated by the bearings and the required power density, would be necessary an accurate study of the problem. Both magnetic and electrical motors are attractive as they are characterized by analogous power density, but the manufacturing difficulties correlated to the "not compatibility" of the ferromagnetic materials with the conventional micro technologies and the operational temperatures that

reduce the properties of the same materials, have pushed to consider, in first analysis, the adoption of electrical devices. The power density scale with the square of the force of the electric field, with the frequency and the rotational speed. Numerous possible configurations for an electrical motor-generator exist; the first choice made by the MIT researchers is an induction machine, because this type of machine does not require a direct contact between the electrical device and the rotor neither the exact knowledge of the position of the rotor [Epstein 2003]. The rotor is composed by a layer of 5-20 μm of good insulator covered by a thin layer of a low conductor (high superficial resistance), while the stator is composed by a series of radial electrodes conductors supported by an insulating layer. The rotating electrical potential is imposed by the external electronics on the stator electrodes and the rotating electric field generates a distribution of charges on the rotor, which is mechanically driven. According to the relative phase between the motion of the charges on the rotor and the statoric field, adjustable from the outside, the device will operate as generator, motor or brake. The torque increases with the square of the force of the electric field and the frequency, but the maximum allowable force is regulated by the dimension of the gap. For the air the maximum is obtained for interstitial values of little micron, so that such machine can theoretically achieve an higher power density than the conventional device with analogous configuration. The frequency is regulated by the external electronic systems and by manufacturing device of the electrodes. Currently 300 volts and a frequency of 1-2 MHz is the maximum value obtained with a 6 mm rotor to producing 10 W with a gap of 3μm and a number of poles much high (beyond 100). To maximize the output power is necessary that the space between rotor and stator is of the same order of the statoric electrodes pitch, that means few μm, but with this type of gap the losses for viscous resistance, considering the machine rotational speed, are extremely high and represent the main source of losses. It is necessary to find a compromise between power density and efficiency. The viscous losses unfortunately represent more than the half of the total ones and limit the efficiency to 40-50%. A magnetic induction machine has the advantage of having less poles and optimal distances rotor-stator very wider (≈10 μm), that produce higher efficiency, around 60%. An ulterior advantage of these devices is that they operate at low frequencies and voltages, and are simpler to build. Currently the greater problems is the thermal resistance of the materials (actually 500 K, but material to working to 800 K have been currently studied) and the rotational speed in conflict with the necessity to insert on the rotor surface a iron layer of about 100 μm. Recently, thanks to new technologies of implantation of the ferromagnetic materials on silicon wafer, a good magnetic induction machine to with interesting efficiency and performances has been realized. As already said, to succeed to adopt a magnetic induction machine respect to analogous electrical devices, implies a greater efficiency, tolerances less limiting and higher manufacturing simplicity. An example of a magnetic induction machine is shown in the figure. The rotor diameter is 10 mm. The machine consists of a two phases stator and 8 poles and of a annular rotor [Epstein 2003]. The electromechanical conversion of the energy is achieved by the interaction of the magnetic field that evolve in the interstice rotor-stator with the current induced in the rotor the displacement of the magnetic wave. The stator consists of two phases composed by planar copper spirals, insert in three-dimensional blocks of vertically laminated ferromagnetic material, all supported by a silicon chassis. The ferromagnetic nucleus has an "onion" configuration, the sheets forms concentric rings, approximately 30 μm thick. This particular shape serves to reduce the induced current losses. The rotor is composed by 2 ferromagnetic ring with a thickness of 250 μm and 2 mm wide covered by a copper layer of 20 μm. The copper is extended over the external beam of the rotor for an ulterior millimetre, to exalt the induced current generation and to increase the maximum torque.

5. Materials

The problems connected to the choice of the materials for a UMGT are referred, partially, to those of conventional machine, in terms of mechanical stresses constraints, operational temperature and manufacturing processes. The materials, generally, satisfy some characteristics penalizing some others, therefore, it is indispensable in the preliminary design to find a good compromise, and not always, the better choice is univocal. It is considered, moreover, that according to manufacturing, the same material can introduce different characteristics. The properties of greater interest for the studied machine are the material absolute specific strength and its resistance to the thermal shocks at high temperatures, the creep and the oxidation, and its derangement characteristics under fatigue cycle. Considering the manufacturing processes and the device dimensions, the first choice for a device MEMS falls on the silicon, thanks the great maturity of the material productive technologies. The silicon also having of the good properties of specific strength and to thermal shock, presents a ductility and a strong "flauge" over the 550°C. This means that I can not use this material in the turbine blade manufacturing. On the contrary, the Silicon alloys appear more interesting, but the manufacturing of these materials is not still mature as well as the silicon ones. The metallic alloys are not able to operate at the demanded high temperatures without cooling or covering, that could create constructive complications. Moreover, the metallic manufacturing does not have a good accuracy. Other advanced ceramic materials, characterized by higher operational temperatures, have insufficient mechanical characteristics to the high temperatures. Adding the fragile behaviour of the ceramic materials, the manufacturing process results problematic and, at the moment, MEMS techniques are accurate only for Silicon and its alloy. Figure 13 put in evidence that the silicon alloys, in this case alumina, can be used at the high temperature, but the Al_2O_3 alloy has lower thermal conductivity and an higher thermal expansion. These characteristics renders the alloy particularly subject to thermal shocks and deformations. Also regarding hardness and elasticity modulus the SiC and Si_3N_4 have higher resistance performances, in particular to bending, and it can be noticed that, also having lower values to low temperatures respect to, for example, the zirconium, such value is maintained approximately constant to the high temperatures and is higher than the other materials. In figure 14 the SiC mechanical properties are maintained, substantially, unchanged with the temperature. The weak of the silicon alloy, like all ceramic materials, is the fragile behaviour, that to large-scale has delayed theirs uses. In large scale components, in fact, the inner imperfections can be in such amounts and largeness that is sufficient the effect of a small extra-solicitations to "prime" the propagation of crack, especially in these materials where the reticulum plans sliding is extremely reduced. For the UMGT order of magnitude, a single piece is composed by a low grains number, so the problem of the structure inner defects is more controllable. The piece surface-volume ratio grows, and will be, therefore, necessary to put greater attention to the superficial defects, prime points for the propagation of crack. From this first comparison, SiC and Si3N4, seem to be the more appropriate materials, thanks to the better behaviour at the high temperatures. There is Recently, adding some elements which boron, aluminium, yttrium and/or relative oxides, meaningful improvements of the mechanical properties have been verified. As previously said, the characteristics of these materials depend on the manufacturing process.

5.1 Silicon carbide (SIC)

SiC presents an optimal material specific strength, a good resistance to the thermal shocks, thanks to its relative high thermal conductivity. In Table 3 the characteristics of the SiC

according to the adopted manufacturing process are listed. The data refer to temperatures between the 20°C and 1400°C and the sources include the main manufacturers companies and some scientific organs, including the NIST (National Institute for Standards and Technologies, USA). Data are, sometimes, discordant depending on the manufacturing process and operational temperature, or because the test and production techniques are not perfectly standardized. In general the worse properties obtained with the Reaction Bonding, the more economic process, and the best ones with the CVD, most expensive one. The Sintering and the Hot Pressing show analogous intermediate characteristics and not too much distant from the CVD. The numerous and reliable data in literature are reported in Table 4. A sintered SiC has been considered, and the result have been completely validated by the NIST.

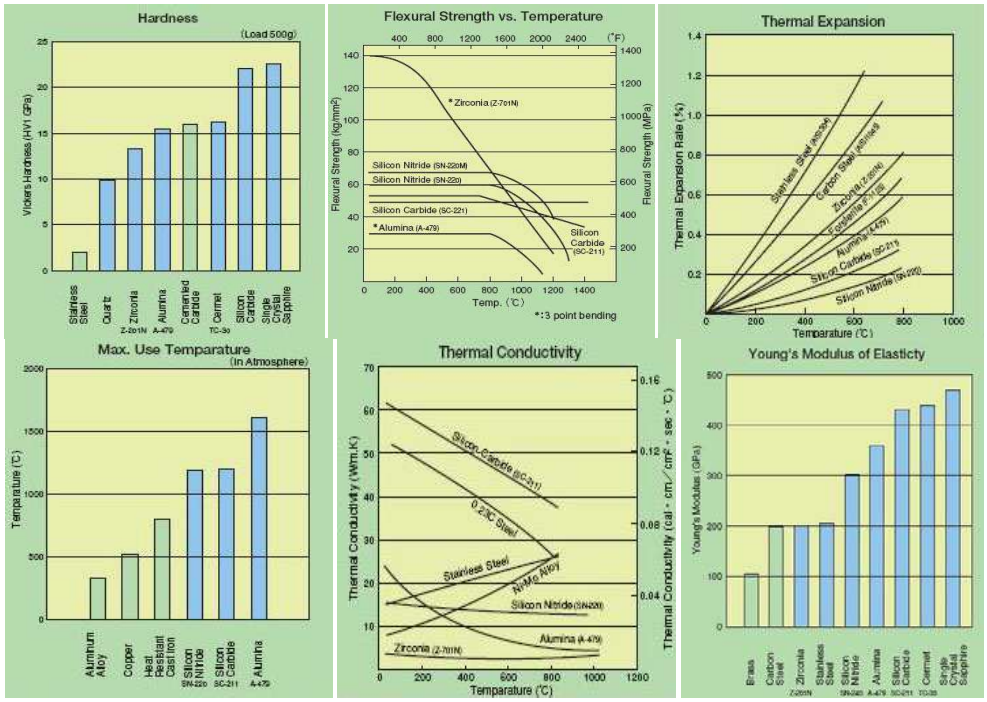

Fig. 13. Materials characteristics

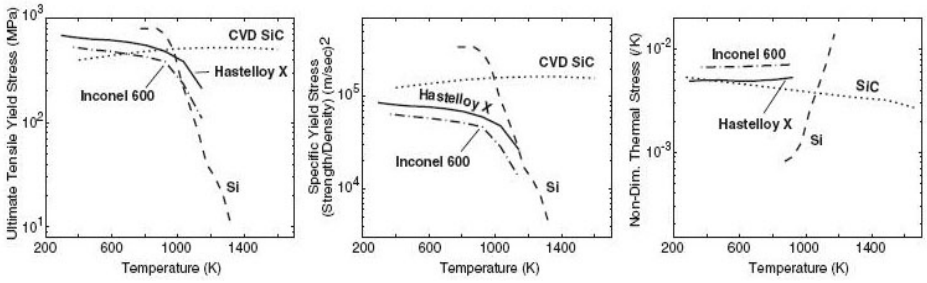

Fig. 14. Materials proprieties at varying of operational temperature [NIST]

SiC	Reaction Bonding	Sintering	CVD	Hot Pressing
Creep Rate Exponent	1.6	1.1	-	0.9
Density [g/cm^3]	2.9-3.1	3.05-3.17	3.21	3.1-3.3
Elastic Modulus [GPa]	275-390	372-450	434-476	380-451
Flexural Strength [MPa]	190-400	359-511	468-575	400-500
Fracture Toughness [MPa m$^{1/2}$]	4	2.6-4	2.7-3.5	3.9
Hardness Vickers [GPa]	22-26	23-26.7	27	21
Max use Temperature °C	1350-1600	1400-1600	1400-1600	1400-1600
Tensile Strength [MPa]	77-310	234-310	220-310	200-310
Thermal Conductivity [W/m K]	110-200	31.3-116	63-300	50-120
Thermal Expansion From 0°C [10^{-6} K^{-1}]	4.3-4.6	4.2-5.9	4.0-4.6	4.3-4.6

Table 3. SiC proprieties at varying of manufacturing process

Percentage in parentheses denote estimated combined relative standard uncertaints of the propriety. For example, 3.0 (5%) is equivalent to 3.0 ± 0.15. Property values in parentheses are extrapolated					
Property [unit]	**20°C**	**500°C**	**1000°C**	**1200°C**	**1400°C**
Bulk modulus [GPa]	203 (3%)	197	191	188	186
Creep rate [10^{-9}s^{-1}] at 300 Mpa	0	0	0	0.004 (17%)	0.27
Density [g/cm^3]	3.16 (1%)	3.14	3.11	3.10	3.09
Elastic modulus [GPa]	415 (3%)	404	392	387	383
Flexural strength [MPa]	359 (15%)	359	397	437	446
Fracture toughness [MPa m^{-2}]	3.1 (10%)	3.1	3.1	4.1	4.1
Friction coefficient[], 0.2 m/s, 5N	0.7 (21%)	0.4	0.4		
Hardness (Vickers,1 kg)[GPa]	32 (15%)	17	8.9	(6.9)	(5.3)
Lattice parameter a (polytype 6H) [Å]	3.0815 (0.01%)	3.0874	3.0950	(3.0894)	(3.1021)
Lattice parameter c (polytype 6H) [Å]	15.117 (0.02%)	15.1440	15.179	(15.194)	(15.210)
Poisson ratio []	0.16 (25%)	0.159	0.157	0.157	0.156
Shear modulus [GPa]	179 (3%)	174	169	167	166
Sound velocity, longitudinal [km/s]	11.82 (2%)	11.69	11.57	11.52	11.47
Sound velocity, shear [km/s]	7.52 (2%)	7.45	7.38	7.35	7.32
Specific heat [J/kg K]	715 (5%)	1086	1240	1282	1318
Tensile strength	250 (6%)	250	250	250	250
Thermal conductivity [W/m K]	114 (8%)	55.1	35.7	31.8	27.8
Thermal diffusivity [cm^2/s]	0.50 (12%)	0.16	0.092	0.079	0.068
Thermal expansion from 0°C [10^{-6} K^{-1}]	1.1 (10%)	4.4	5.0	5.2	5.4
Wear coefficient (log10) [0.2 m/s, 5N]	- 4.0 (5%)	-3.6	-3.6	**…**	**…**
Weibull modulus []	11 (27 %)	11	11	11	11

Table 4. Sic proprieties [NIST}

5.2 Silicon nitrate (Si_3N_4)

The silicone nitrite is a material much industrially diffusing. In Table 5 the main characteristics of the Si_3N_4 are reported, according to the manufacturing process, for a temperature within 20°C and 1400°C. Data, relative to CVD operations, are not available, because for such material is only used to generate protecting films, not for solid pieces

Si_3N_4	Reaction Bonding	Sintering	CVD	Hot Pressing
Creep Rate exponent	1.7	1.1	-	1.2
Density [g/cm³]	2.3-2.6	3.2-3.27	-	3.1-3.31
Elastic Modulus [GPa]	155-200	245-310	-	175-320
Flexural Strength [MPa]	190-338	70-703	-	146-930
Fracture Toughness [MPa $m^{1/2}$]	2-3.6	4.3-6	-	3-8
Hardness Vickers [GPa]	10	14.8-15.7	-	13.9-15.9
Max use Temperature °C	1200-1500	1000-1500	-	1200-1500
Tensile Strength [MPa]	140-170	140-576	-	140-726
Thermal Conductivity [W/m K]	10-16	26-30	-	15-42
Thermal Expansion From 0°C [10^{-6} K^{-1}]	2.9-3.3	3.1-3.5	-	2.7-4.3

Table 5. Si_3N_4 proprieties

creation. From a data analysis, the properties of the Si3N4 are strongly variable, also presenting higher values than the SiC ones. In effects the silicon nitrite has optimal characteristics to low temperature, but it degrades quickly with the temperature increase. To high temperatures, also maintaining a good behaviour, does not reaches the SiC values. In this case, it can be noticed as the Reaction Bonding does not allow to obtain good property because of the achieved lower density than the theoretical one: the porosity is too much high.

5.3 Tenacity, fracture toughness, creep, time to failure

The fragile behaviour of the ceramics focuses the study of the mechanical characteristics on the field of the mechanics of the elastic linear fracture. The design, in this case, is difficult because the microcrystalline structure of the ceramics introduces intrinsic imperfections in the mold preparation and edging processes, that render the material properties extremely variable. A greater limit of the ceramic materials is the low fracture toughness K_{IC} and, consequently, the greater probability of structure collapse due to the crack propagation. The critical crack length "l_c" represents the dimension which the phenomenon increase and becomes spontaneous and irreversible. This event is not correlated to the operational environment but linked to the produced energy during the inner material tensions displacement. This largeness represents the maximum tolerable dimension of a crack in operational conditions, and determines the structure lifetime. Beginning from the energetic criterion of Griffith [Frechette] the simplified formula can be written:

$$K_{ic} = \sigma\sqrt{\pi \cdot l_c} \tag{24}$$

Once σ and K_{IC} are known (Table 4 e 5) the SiC critical crack length can be calculated:

$$\sigma = SU_1^2\rho_m = 133.2 \text{ MPa} \Rightarrow l_c = 172 \text{ µm} \tag{25}$$

for Si_3N_4:

$$\sigma = SU_1^2\rho_m = 137.6 \text{ MPa} \Rightarrow l_c = 420 \text{ µm} \tag{26}$$

The silicon nitrite have a better tenacity, but of a lower value (140 MPa, Table 5) of the maximum permissible stress to traction at high temperature, value that appears insufficient to assure adequate safety margins. It can be noticed as the critical length, at this scale, is an

order of magnitude lower than the blade dimensions., and two orders of magnitude higher than the device accuracy, that evidently would lose its functionality with a crack "so large". Recent studies, aimed to improve the tenacity of the ceramic materials, thanks to the addition of some additive (Al, B and C), to clearly increase the K_{IC} till values (for SiC) of 9. It can be assumed that the machine lifetime, subordinate to the maximum static stress (as previously calculated), is higher than to 10^4 hours if SiC is used (Figure 15), while is ~600 hours for the Si_3N_4 (Figure 16). In both cases the structure deformations, due to the sliding, are of little µm, therefore negligible because the design tolerances that are of about 10 µm.

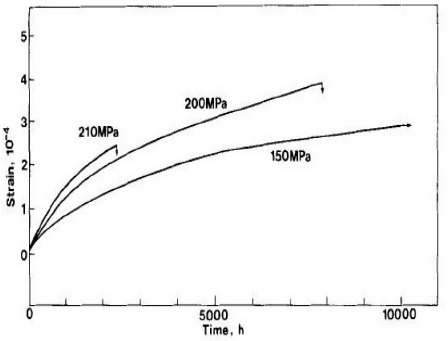

Fig. 15. Alumina SIC alloy creep curves at 1400°C [NIST]

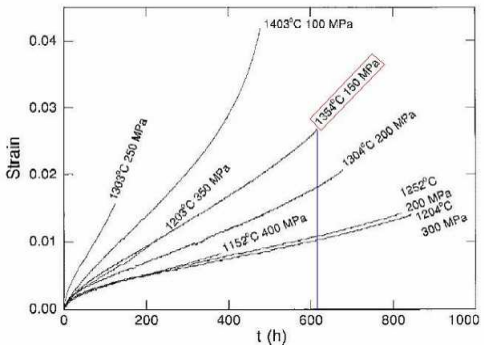

Fig. 16. Si_3N_4 creep curves [NIST]

The mechanism of complete structure failure the under a stationary cargo has had to the interaction between sliding and defects existence, to the speed of crack propagation. Both properties depending on the manufacturing process.

In static conditions, the solicitation, where, superficial carvings or micro cavity between grains, are present, generates a crack advance along the grain edges, the material weaker point. Once reached the critical length, the structure fails and this happens in a determinate time, defined Time to failure; a stress σ_{th} of minimal threshold exists, necessary to prime the process of crack propagation. Under these conditions, it seems that the piece is capable to resist for an indeterminate time. For silicon carbide it has been extrapolated (Figure 17): σ_{th} = 165 MPa to traction to 1400°C. It can be noticed that for values higher than the threshold one,

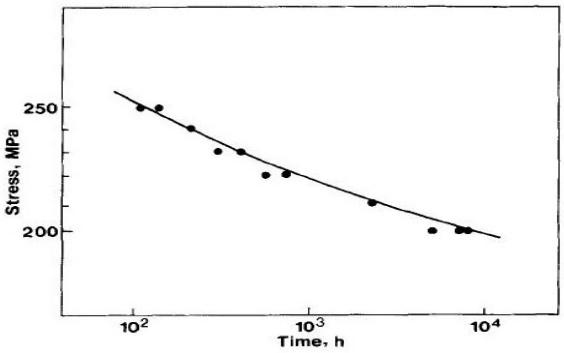

Fig. 17. SiC *Time to failure* at 1400°C [NIST]

the lifetime is maintained to 10^4 hours. For Si_3N_4 this value is lower: $\sigma_{th} \approx 150$ MPa to traction at 1300°C; Figure 18 shows how this value rapidly decrease at the temperature increasing. Particularly interesting is the fatigue behaviour, that it is one of the main mechanisms of priming and lengthening of a crack, and in for ceramic materials represents the determining factor of the lifetime. In the fragile materials is distinguished between static fatigue and cyclical: the first one is related to the supported load, with variable conditions of temperature and in oxidating atmosphere, while the second, the most meaningful one, is determined by variable solicitations conditions. The fundamental law that regulates the material fatigue lifetime is famous as law of Paris, the expresses the crack propagation velocity in "N" number of cycles:

$$\frac{da}{dN} = C\Delta K_i^{\ m} \tag{27}$$

The constants C and "m" is closely correlated to the material, while the ΔK_i represents the variation of the stresses intensity factor (That means it is correlated to the structure applied solicitation). In the metals the exponent is small (m between 2 and 4) and an increase, as an example of a factor 2, the $\Delta\sigma$ applied to the machine reduces the component life-cycles of a order of magnitude, acceptable during design procedures.

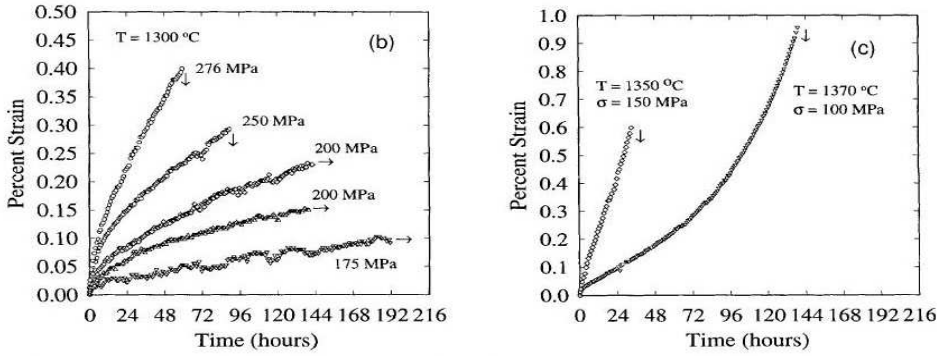

Fig. 18. Si_3N_4 lifetime at varying of solicitations and temperature [NIST]

For the ceramic materials, the exponent is much higher (m > 20) and it is enough a factor 2 to modify the he component life-cycles at least six orders of magnitude. It is possible but to take advantage, in the preliminary design phase, of the threshold value of the ΔK_i, that defines the variation of the stress intensity factor, and consequently, the value of the stress under of which the fatigue is negligible. Such value is usually around 50% of the K_{ic}; in the event of the SiC reinforced with Al, B, C the data are represented in Figure 19. Operating under this threshold value, it is possible to reduce the influence of the fatigue on the machine lifetime to a secondary parameter, even if, some factors which the corrosive atmosphere or the inner disposition of the micro cavities can limited the really usable an allowable ΔK_i. The available data for the UMGTs, actually under investigation, unfortunately, are not sufficient to determine the influence of the fatigue on the machine.

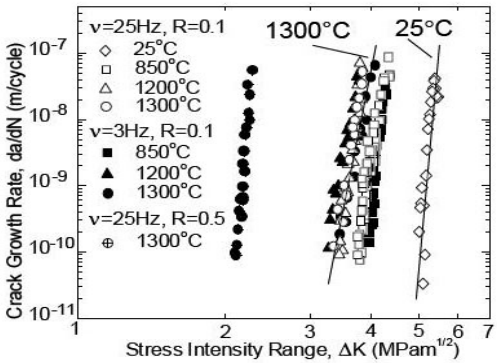

Fig. 19. Si_3N_4 Stress intensity range

5.4 Ceramic materials

The ceramic materials are interesting for structural applications as they are thermally stable and not so heavy. In fact, since between their atoms create covalent or ionic bond, such materials generally have a high chemical inertia, a high elastic modulus and a remarkable hardness, also to temperatures over 1000°C. The same chemical bonds that give them interesting characteristics are also responsible of their fragile behaviour. They do not allow to the crystalline plans to slide ones regarding the other, and do not allow the material plastic deformation. Consequently the ceramic material presents a typical fragile fracture: without some warning, with a highest crack propagation velocity. Such behaviour is described using the Griffith law:

$$\sigma = \frac{K_{IC}}{\sqrt{\pi a}} \tag{28}$$

To render ceramic a reliable material (or better to increase its Weibull module) it is necessary or increase the value of its critical stresses intensification factor or decrease the inner defects dimensions. In the first hypothesis it needs to modify the microstructure by new insertion of "new phases" in the matrix, in the second needs to optimize composite "processing" of and to take care the superficial finishing.

5.4.1 Weibull statistic

The design of ceramic components are based on three types of approach:

- an *empiricist* approach, based on the iterative tests execution of that finish when the member satisfies the properties demanded. Sometimes, if the modelling and the previewing, this is the only solution;
- a *determinist* approach, in which it is attempted , by mathematical models, to preview the material resistance behaviour. This approach is correlated to the FEM analysis, and satisfied with the metals but sometimes it is inadequate for the ceramic ones, especially in the design loaded by critical stresses;
- a *probabilistic* approach: it is assumed that a data volume of ceramic material loaded by uniform stress breaks for effect of the defect of greater entity (approach of Weibull)

Weibull (1939) was the first one to introduce, through an statistics analysis, the concept of breach probability. In its model the member is considered as "a chain" constituted from N meshes: the failure of this chain when the destructive breakdown of a single mesh occurs, that weaker one. Such event is independent by the other possible events (failures). In statistical terms, the reliability of the chain is calculated as the product of the reliability of each mesh. The concept is perfectly suitable to the examination of a ceramic volume. To such purpose the experimental observation indicates that the Failure Probability $P_{f,u}$ is given by:

$$P_{f,u}(\sigma) = 1 - e^{-\left(\frac{\sigma}{\sigma_0}\right)^{\beta}} \tag{29}$$

in which σ_0 and β are material constants. According to this model the probability is zero for null tension and unitary for tension sufficiently elevated. The A_u reliability of the of volume element, equal to the complement to 1 of the probability, is:

$$A_u(\sigma) = e^{-\left(\frac{\sigma}{\sigma_0}\right)^{\beta}} \tag{30}$$

According to the "chain" model, the $A_{V(\sigma)}$ reliability, of a component of volume V subject to a uniform stress σ, is equal to the product of the reliabilities of the unitary elements that compose it, that is:

$$A_V(\sigma) = e^{-V\left(\frac{\sigma}{\sigma_0}\right)^{\beta}} \tag{31}$$

So failure probability is equal to:

$$P_{f,V} = 1 - e^{-V\left(\frac{\sigma}{\sigma_0}\right)^{\beta}} \tag{32}$$

To this the function corresponds to the probability density of failure, expressed by the relation (32). The defined formula is indicated as 2 parameters Wiebull distribution. The parameter β is called "Weibull modulus" while the parameter σ_0 is a scaling parameter. If the tensional state is not uniform, the reliability of the component of volume V is given by the product of the single constituent unit reliabilities of the total volume. Finally, it can be noticed that β modulus expresses a "simple probability" of the ceramic material behaviour.

$$p_r(\sigma) = \frac{\partial P_{r,V}(\sigma)}{\partial \sigma} = \frac{\beta V}{\sigma_0}\left(\frac{\sigma}{\sigma_0}\right)^{\beta-1} e^{-V\left(\frac{\sigma}{\sigma_0}\right)^{\beta}} \quad (33)$$

5.5 Monolithic materials and composites

The monolithic ceramic materials, that is without reinforced fibres are not adapt for applications to high temperature, due to the low resistance to the thermal shocks and for fragile behaviour. Since than ten years the research is being focused on ceramic materials that are constituted by ceramic reinforced matrices with ceramic fibres. The composites present a better tenacity and fracture toughness. We can notice that, also having chosen a matrix and a phase to increase its tenacity, to put together these elements and to create a composite with sufficiently low defects is not so simple. For composites with polymeric and metallic matrix, the problem is not banal: the matrix can be, in fact, brought to the liquid state, and consequently during the cross-linking and the cooling processes, the amount and the dimensions of the vacancies are rather small. Different is the case of ceramic composites. The matrix cannot be melt, because (moreover the technological difficulties linked to the manipulation of the liquid phase at temperature over 2000°C) or it is decomposed before melting or its fusion temperature are much high to react with the tenacity phase. The only method to increase the matrix density, is the sintering process, that can be defined schematically as a succession of hot transformations of the material structure that take advantage of mechanisms of gaps and species gaseous diffusion: in such a way a gas expulsion contained in green ceramic material is provoked, eliminating the excessive porosity and increasing the material compactness.

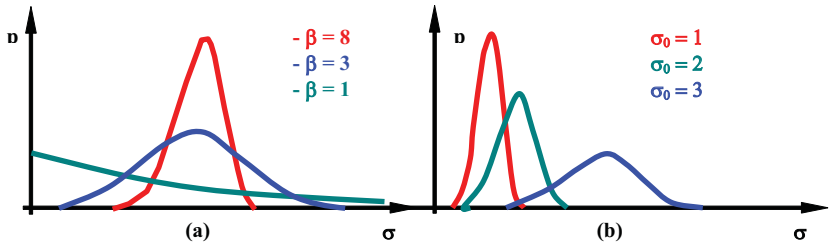

Fig. 20. β (a) and σ (β) distribution at varying of probability density

The model of the contact spheres elaborated by Frenkel and Kuczynski in 40s, explains metals and glasses densification process (the light violet sphere indicate the glass phase increase). This model is extended by Kingery to the sintering for the solid state diffusion for the ceramic materials. This process starts from the ceramic powders, to which has to be added a second phase, often constituted by particles with dimensions of some micron and lengthened shape. All it must then be heated to high temperature to prime the sintering process. It is opportune that the particles dimensions of the two phases can be comparable, to avoid that the larger particles stop or delay the process, working as "rigid inclusion" and producing a low density material with great vacancies amount, with poor mechanical properties, even if the K_{IC} has been improved by the presence of the new phase. Generally, to produce ceramic composites an "oxidic" matrix can be used, like the alumina, the zirconium, ecc. Moreover some matrix with essentially covalent bond can be used, as an example the silicone nitrite, boron nitrite or aluminum, the silicon carbide and others. Between

the oxides based matrices, the alumina is most used. It has good mechanical properties, but its main propriety is the resistance to the usury and to the oxidation; less good are its creep resistance. The tenacity and the heat conductivity are lower. Other materials can be remembered, thanks of their wide use, like the yttrium, zirconium, and various carbides and nitrides. Both monolithic and composites materials, even if characterized by elevated stability, are subject to several forms of structural decay if loaded at high temperature.

5.5.1 Property of the ceramic materials and high temperature behaviour

The properties of the ceramic material at temperatures over 1600°C are analyzed here below. For the applications in study, they are:

1. oxidation resistance;
2. structural resistance to traction/compression and shear stresses;
3. creep;
4. tenacity;
5. fatigue.

5.5.1.1 Oxidation resistance

Many structural applications to high temperature demand the exposure to highly oxidant atmosphere: the thermal stability and the oxidation resistance to the oxide materials become of fundamental interest. A comparison of parabolic rates of oxidation for not oxidic ceramic materials is introduced in Figure 21. In general, an acceptable rate of oxidation is attested around 10 $\mu m^2/h$; this is equivalent to assert that the material produces 100 μm of oxidized slags in 1000 hours. As previously described, the great part of carbides, borides and nitrides, oxidize to rates that exceed of several orders of magnitude this threshold value, and consequently they can not be used in the long term structural applications to high temperature. Only the silicon nitride Si_3N_4 and carbide SiC are able to maintain the previously determinate value to the temperature of 1600 °C. Although the great part of the oxidic ceramic materials are considered stable in a full oxygen atmosphere, the phases interfaces can be oxidized in presence of an oxygen gradient; as an example, if stable ternary oxide, ABOx, are subject to an oxygen gradient and if the relative diffusion coefficients to the three elements are in the relationship $D_A > D_B > > D_0$, the crystal will rich of AO on the side of the greater gradient.

5.5.1.2 Traction/Compression and shear structural resistance

Many polycrystalline ceramic materials quickly lose their characteristics of structural resistance at high temperature. Hillig indicates that the resistance of fragile materials would have to decrease proportionally to the 3/2 of the T/T_{melt} ratio (T_{melt} is the melting temperature of the materials) and that the value would have decrease of the half approximately if the environment temperature is equal to 0.5 T_{melt}. This behaviour is the result of the diffusion mechanism control of the particles that dominate the processes of deformation to the high temperature. A schematic diagram of the resistance limits correlated to the mechanisms of fracture and creep in the ceramics is shown in Figure 24. To high temperatures many materials show ductile behaviours; this involves that their properties of resistance immediately are controlled by creep phenomena. Consequently, the advance of the micro-crack in the material is regulated by the creep. In the table 6 and Figure 23 the resistance limits and the fields of application of several ceramic materials are shown s: for

many applications is necessary not to exceed tensions of the order of 10^2 MPa (typically 150 MPa) to safety reasons. No ceramic materials shown in figure seem able to support this tension to approximately 1600 °C; consequently the composites materials reinforced with fibre are the only ones that allow reaching such design specifications. The titanium boride they seem to be of the possible candidates to reinforce of oxidic matrix, having excellent resistances to the high temperatures, but highly oxidable even if they are included in the matrix.

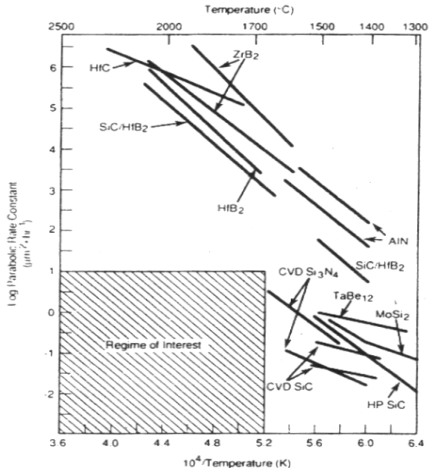

Fig. 21. Oxidation curve

Also the pure silicon carbide introduces an adapted resistance in the temperature range of interest, but the structural SiC and its fibres are typically lacking the necessary purity to obtain high levels of resistance, and consequently, present meaningful proprieties losses to 1200°C. A better quality in the realization of silicon carbide fibres is being obtained with the new formation processes to high temperature. The oxidic ceramic materials, on the other hand, do not present the necessary resistance in high temperature atmospheres. Meaningful improvements have been obtained through the increase of the hardness of the solution or the control of the precipitate (above all zirconium), but the allowable stress have been always maintained lower than 150MPa. The sapphire (mono crystalline alumina) shows the necessary degree of resistance if oriented in opportune way during its cooling, but the more amazing result have been obtained using a two-phase material apt to receive ulterior oxidic phases: the eutectic system Al_2O_3/YAG, is capable to support stress of about 250 MPa to 1650°C. Studying this material, it appears clearly, that in the ceramic the crystals orientation is most important and, therefore, the direction of solidification of the green ceramic.

5.5.1.3 Creep

Figure 24 illustrates that creep is the dominant dynamic process to the high temperature, as well as that it is assumed as design criterion in any structural application. The creep rates must be of the order of 10^{-8}/s or lower for long term applications; to obtain these resistant levels, a creep resistance fibre must be deposited into a less resistant matrix. It is obvious that the polycrystalline ceramic fibres are not able to supply an adequate creep resistance for such matrix. The oxidic and monocrystalline fibres analyzed by Corman seem to be more promising. As an example, it can be noticed the interesting behaviour of the mono

crystalline yttrium-alumina-garnet ($Y_3Al_5O_{12}$): this fibre present an interesting creep resistance (in our application field), and, being to cubical material, its creep advancing rate is independent to the direction of its crystals; for this reason, the fibres having such structure, present a better resistance to complex stresses states.

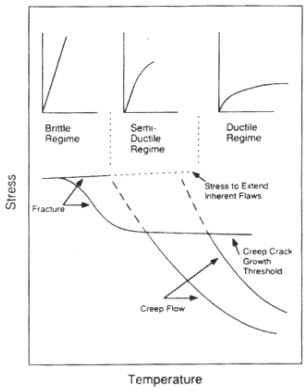

Fig. 22. Stress/temperature diagram

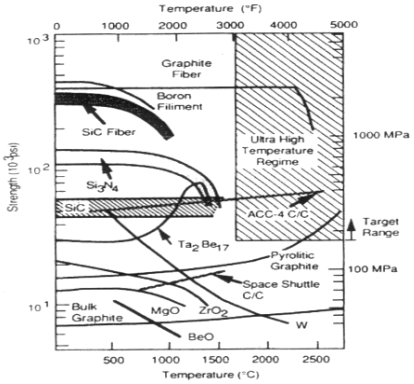

Fig. 23. Application field

Material	Temperature(°C)	Yield Stress(MPa)
Al_2O_3 - prismatic	1600	80-120
Al_2O_3 - pyramidal	1600	200-300
ZrO_2 (4.5 mol% Y_2O_3)	1400	550
ZrO_2 (9.4 mol% Y_2O_3)	1400	160
ZrO_2 (9.4 mol% Y_2O_3)	1600	40
ZrO_2 (18 mol% Y_2O_3)	1400	275
TiB_2	1600	> 800
TiB_2	1900	500
SiC	1600	350
WC	1600	100

Table 6. Resistance characteristics

It is not so easy, on the contrary, to preview the behaviour to creep of reinforced composite ceramic; a dominant parameter to take under control, in such composites, is fibre aspect ratio.

The stationary creep phenomenon on formed ceramic materials is analogous to that one shown for the metallic ones, above all, in relation to the dependency by the module of applied stress. Cannon shows how the exponent (n) in the formula (36) varies within 3 to 5 in the "dislocation climb" and within 1 to 2 when the diffusion mechanisms are active. It is assumed here that the behaviour to creep of a ceramic fibre and its matrix can be described from a common "power law" expression of the type:

$$\dot{\varepsilon} = A\sigma^n \exp\left(-\frac{Q}{RT}\right) \tag{34}$$

where the composite deformation speed $\dot{\varepsilon}_c$, and the σ_C stress, are weighed with the volume fraction of the two phases. The composed stress σ_C can be correlated to creep through the following formula:

$$\sigma_c = \frac{\sigma_{fo} V_f \dot{\varepsilon}_c^{1/n}}{\dot{\varepsilon}_{fo}^{1/n}} + \frac{\sigma_{mo} V_m \dot{\varepsilon}_c^{1/m}}{\dot{\varepsilon}_{mo}^{1/m}} \tag{35}$$

where, σ_{fo}, ε_{fo}, σ_{mo}, $\varepsilon_{fo,}$ are obtained from material empiric relations, and "m" and "n" are the stress component for the matrix and fibres respectively. This equation allows calculating demand stresses to support a stationary creep speed in a continuous composite, being assumed that both fibres and matrix are sliding to the same speed and without distortions on the phase interfaces.

5.5.1.4 Tenacity

Before using a fragile material in a structural application the resistance limit to thermal shock, damaging from impact and fast fracture for cracking advance must be indicated. As previously shown, the creep is the process of dominant deformation when the sliding tension is lower than the necessary one to prime unstable crack advancing. The intensity of

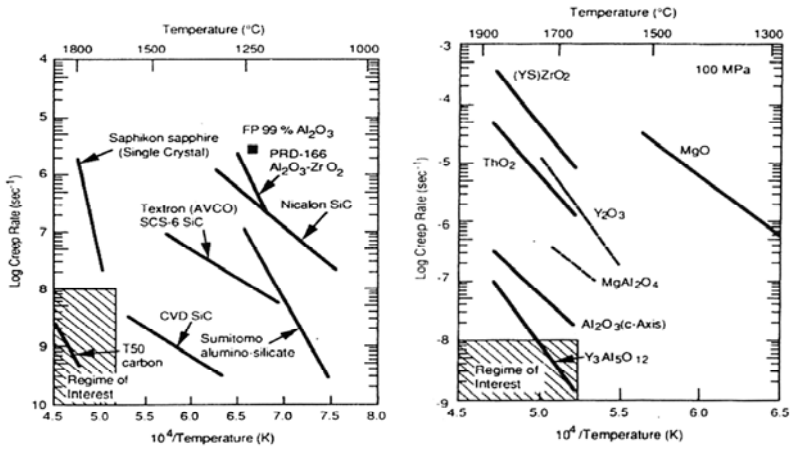

Fig. 24. Creep behaviour

the applied and localized stresses shows different increases in relation to the crack length; this produce a ductile behaviour in the material when the stress, K_m, is lower than the limit stress, $K_{th.}$ The tenacity is the result of the applied traction on the fracture of the matrix by same fibres behind the fracture line: the friction of the fibres to the sliding of broken fibres opposes resistance in the crack matrix. The table 7 reports the studied structural ceramic composite properties.

Composite reinforcement/ Matrix	Flexure or Bend Strength (MPA)		Creep @ 100 MPa s^{-1}	R.T. Toughness MPa $m^{-1/2}$	Fatigue	Oxidation resistance
	R.T.	Elevated Temp.				
Reinforcements	----------	----------	----------	----------	---------	----------
Carbon	2000-4000	≈2500 @ 2300°c	10^{-11} @ 1600°C	U	U	Catastrophic
TiB_2/TiB(C)	670-1560	900@ 1000°C	U	U	U	Poor
Sic (CVD)	3200	1200 @ 1400°C	$3 \cdot 10^{-9}$ @ 1600°C	U	U	Good
SiC (polymer)	1900	1050 @ 1400°C	$5 \cdot 10^{-9}$ @ 1400°C	U	U	Good
C-axis Al_2O_3	1400-3000		10^{-9} @ 1600°C	U	U	Stable
C-axis BeO	U	≈40M @ 1000°C	10^{-9} @ 1750°C	U	U	Stable
YAG	U	U	$5 \cdot 10^{-10}$ @ 1600°C	U	U	stable
Nonoxide/Nonoxide	----------	----------	----------	----------	---------	----------
BNp/AlN-SiC		28 @ 1530°C	U	U	U	Fair to 1600°C
SiC/SiC	350-750	U	U	18	U	< 10□m^2/h (1600°C)
SiC/HfB_2	380	28 @ 1600°C	10^{-5} @ 1600°C	U	U	12□m (2000°C)
SiC_p/HfB_2-SiC	1000	U	U	U		5% wt gain (1600°C)
SiC/$MoSi_2$	310	20 @ 1400°C	U	≈ 8	U	< 10 m^2/h (1600°C)
ZrB_2pl/ZrC(Zr)	1800-1900	U	U	18	U	U
20vol% SiC/Si_3N_4	500	U	U	12	*	Good to 1600°C
Nonoxide/oxide						
SiC/ZrB_2-Y_2O_3	U	16 @ 1530°C	U	U	U	Poor
TiB_2/ZrO_2	U	U	U	U	U	Poor
SiC/Al_2O_3	600-800	U	10^{-5} @ 1525°C	5-9	U	Poor
30vol% SiC/ZrO_2	650	40 @ 1000°C		12	U	Poor > 1200°C
Oxide/oxide	----------	----------	----------	----------	---------	----------
Al_2O_3/mullite	≈180		U	U	U	Dissolution reaction
Al_2O_3/ZrO_2	500-900		U	U	U	Stable
YAG/Al_2O_3	373	198 @ 1650°C	U	4	U	Stable

U = unknown
* = 0.22mm crack after 50000 cycles @ 42 MPa in compression

Table 7. Ceramic material proprieties [NIST]

5.5.1.5 Fatigue

The today's design strategies are based, first of all, on the tenacity and resistance of the material. The behaviour to cyclical fatigue, thermal and mechanical one, must be enclosed as

an essential element in the design analysis. The *thermal fatigue* takes part on every material under re-heating and cooling cycles. The thermal shock is the effect and it is present every time that a material is not constantly heated or it is not held to a constant temperature. Naturally, when a material is heated in a furnace, above all if its heat conductivity is low, and is quickly heated, or vice versa, quickly cooled, it creates thermal gradient in the material. In these conditions every such material are characterized by embrittlement, thermal fatigue, micro fractures, crack, etc. that, in the long run, produces a thermo mechanical failure. These important considerations have to be mentioned, especially during the preliminary design phase. In fact it is not enough to consider the maximum temperature of resistance of a material or the mechanical resistance, but all the problem boundary conditions that indicates the better choice of the material to use. The *mechanical fatigue* is caused by "slow crack growth" (SCG) mechanisms that must be analyzed for nominal load conditions. In spite of the acquaintance of the mechanism, the device lifetime prevision is based on empiric correlations for the crack rate. Generally a "power law" is adopted, whose main advantage resides in the mathematical model simplicity:

$$v = \frac{da}{dt} = A\left(\frac{K_I}{K_{IC}}\right)^n \tag{36}$$

where "v", "a" and "t" are the crack rate, its characteristic length and the time respectively. K_I and K_{IC} are the stress intensity factors (effective/critical). "a" and "n" are parameters depending on the material and the operational atmosphere. The lifetime (t_f) depends essentially on the applied stress (assumed constant) and on the K_{IC}:

$$t_f = D\sigma^{-n} \qquad D = f(K_{IC}; A; n) \tag{37}$$

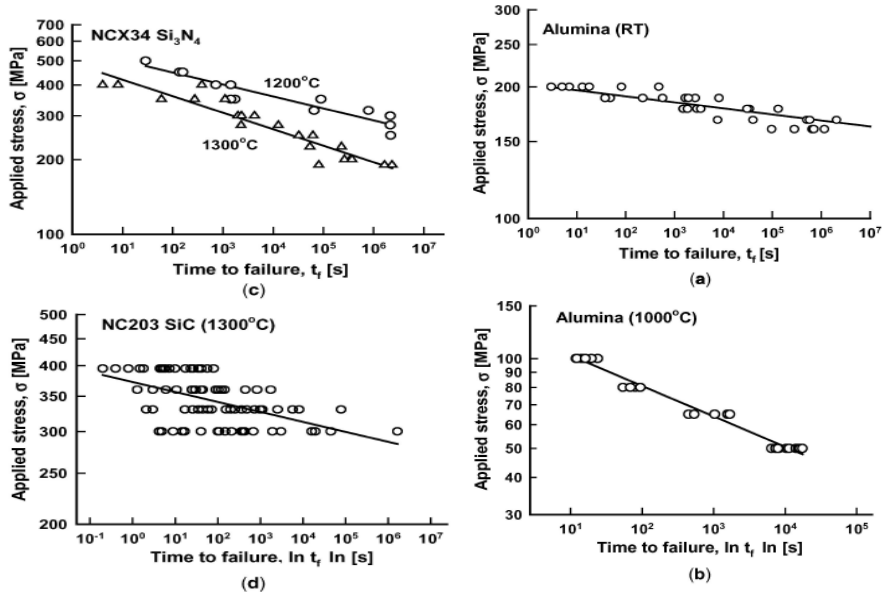

Fig. 25. Ceramic materials Fatigue diagrams

5.6 Metallic materials

5.6.1 Stainless steel alloy

Low C tenor alloy (except some martensitic steels), or better Fe-Cr or Fe-Cr-Ni alloy, with Cr percentage varying from the 12 to 30% and of Ni from the 0 to 35% (main characteristic is the corrosion resistance). Such characteristic is due to the passivation property that such steels, in oxidation conditions, have (that is capacity to create an oxide film of extremely thin dimensions whose characteristics remarkably according to change the chemical composition of the alloy, of the heat treatment, the structural composition, the superficial stress state) . Normally they are subdivided in following the three classes:

- Martensitic steel ;
- Ferrite steel;
- Austenitic steel.

The martensitic steels have the critical points and are submitted to heat treatment; they have higher mechanical characteristics in comparison to the ferritic and austenitic ones, but lower corrosion resistance. The ferritic steels, instead, do not possess the critical points, can only be submitted to re crystallization annealing treatments; they have good resistance to oxidation at high temperature, as well as more elevated how much greater are the chromium content. the austenitic steel are, between the stainless steel, those mainly produced. They have elevated corrosion resistance in numerous atmospheres; they are submitted to heat volatilization treatment (hardening of austenitic steel) to melt, in the austenitic matrix, the Cr carbides (their presence decrease the corrosion material resistance). For this same reason the C tenor has to be held to low values. Besides these three classes are the stainless steel hardening by precipitation, with high mechanical characteristics, whose corrosion resistance, also being lower than the austenitic types, is higher than martensitic ones. Hardening process derives by the precipitation insoluble phases dispersed during the aging process. Between this type of steels we remember:

1. quality steels for mechanical constructions (UNI 3158);
2. high tensile steels (UNI 4010);
3. usury resistant steels (UNI 3160);
4. heat resistant steels (UNI 3159);
5. corrosion resistant steels (UNI 3161);
6. creep resistant steels (UNI 3608).

5.6.2 Refractory alloy

To this group belong the high temperature resistant metallic materials. They are used in gas turbines manufacturing, reaction engines, inner parts of furnaces. They must present a good corrosion resistance at high temperature (the oxidation phenomena at high temperature) and be capable to support attacks from combustion ashes (in particular S, V and its derivates, contained in the ashes), and good creep strength (creep-fluage). They are distinguished in:

- Fe base alloy;
- Ni base alloy;
- Co base alloy.

The refractory steels are used for those products whose main characteristic is the resistance to hot gases and residual of combustion, at higher temperature than 550 °C. In European code for these materials is EURONORM 95.

5.6.3 NICHEL alloy (Ni)

Melting point is approximately 1455 °C. The Ni, in steels alloy, reduces the grain dimensions, increases the depth of hardening and renders them less sensitive to the low temperatures fragile failure. The Ni can be bond with numerous metals (particularly with Fe, Cr, Cu). The Ni- Fe alloys can be:

- With low expansion coefficient or controlled expansion as the Invar; these alloys find applications in the fabrication of physical measurement device, bimetals and equipment for lowest temperatures;
- alloy with constant elastic modulus used for clocks springs, frequency regulators;
- alloy with special magnetic characteristics (non-magnetic, low and high constant permeability);
- Magnetic resistance alloy, for transducers;
- Cr or Co alloy, resistant to the heat;
- Cu alloy, resistant to sea water and to many chemical compounds (Monel-Metal).

5.6.4 COBALT alloy (Co)

It is used in metallurgy with Fe, Ni, Mo, W and other metals for the production of refractory alloys, steels for tools and alloys for permanent magnets. It is a constituent of maraging steels.

5.6.5 TITANIUM and TITANIUM alloy (Ti)

Ti is recently used in the industrial manufacturing but its utilization still is limited, due to the high fabrication cost. The main properties of this metal and its alloys are the oxidation resistance also to 400-450 °C and higher mechanical characteristics both cold and hot environment. Its low density (4,54), has as consequence an high σ_m/p.sp ratio. The melting point is 1672 °C. These characteristics of pure Ti and its alloys are a lot influenced by the inner contained gas and, in particular, by the H. The value does not have to exceed the 0,0125% to avoid a dangerous embrittlement. The Ti alloys find application in the fabrication of supersonic vehicles, the aerospace constructions and in particular in the missiles.

6. Manufacturing technologies and process

The UMGT design is strongly limited by the available technologies. The micro manufacturing introduces a several problems in the development of every single part of the device. All studies have bring to adopt as manufacturing techniques the DRIE (Deep Reactive Ion Etching) and the Wafer Bonding, diffuse and by now widely mature, add to Micro Reaction Sintering, a new process based on the HIP (Hot Isostatic Pressing), already experimented for the fabrication of micro turbines and capable to realize machines with an accuracy of the order of the μm, in small series and with contained production costs.

6.1 DRIE (Deep Reactive Ion Etching)

This technique essentially consists in etching wafer of base material, usually silicon microcrystalline, through a plasma beam. Considering that a wafer has a diameter between 100 and 300 millimetre, it is possible, at the same time to produces numerous devices, in parallel, as shown in Figure 26.

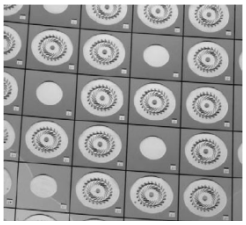

Fig. 26. Series of nano devices on a single wafer [Epstein 1997]

Initially the wafer is covered by an oxide and by a photo resistant film, on which a so-called "mask" is transferred through optical methods, a model in black and white with the geometry to recording. The transfer is realized bombing with ultraviolet rays a glass plate to contact directed with the wafer, on which the mask is applied. Geometry is so "developed" on the photo resistant material as if it were a normal photographic film. Finally and the piece is "cooked". After the "development", some oxide exposed parts remain, that are removed using solvents, leaving some area covered by the mask and some zones uncovered by silicon material. The piece is, then, etched, but the speed of the oxide etching is 50-100 times lower than of the silicon one. At the end of the procedure, the extruded initial

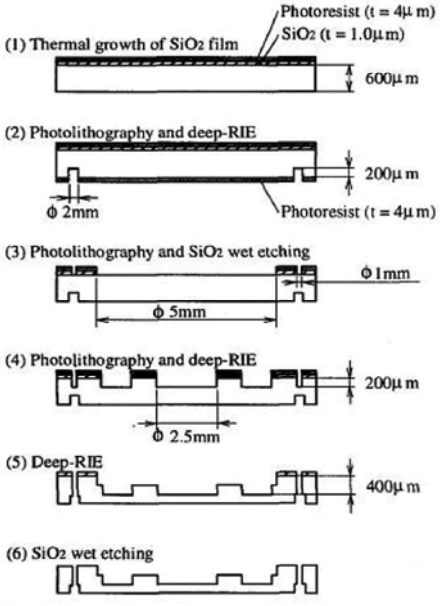

Fig. 27. DRIE manufacturing process phases

geometry is obtained. Several materials and techniques exist to produce the photo resistant mask, and SiO_2 is the most diffuse used oxide. The etching plasma beam can be composed by ion mixtures of varied nature. The process is described in Figure 27. Numerous manufacturing companies have developed particular and sophisticated machine capable to deeply etching with extreme precision, even if the adopted process is usually the Bosch patented one. Moreover several machines and device commercialized from the Alcatel, are capable to achieve an etching speed of 20 μm/min with aspect ratio of 60:1, but with the possibility to arrive till 100:1 with an ulterior cost increase. Practically, without excessive expenses, the stamps for the turbine in less than an hour and for the compressor in about 30 min could be recorded, without the necessity of successive manufacturing, since this technique has an accuracy of the order of the μm. Add the possibility to obtain tapered shovels and etchings of about 0,25 μm. The disadvantage of this technique is that simply extruded geometries can be only obtained, but already is being worked to create masks in greys tonality to producing more complex forms and shape, that could allow to have a height of the channels variable, with the consequent possibility to adopt thin profiles for the turbo machines.

6.2 Wafer bonding

This technique allows to create complex structures joining, using different other materials which the glass, wafers of already micro etched silicon. The fusion between the several parts is superficially obtained by cooking the parts, in presence of a strong cross-sectional electrostatic field that crosses the pieces interface. This system creates an alloy; the high temperatures strengthen the bonds (anodic fusion). In alternative, it is possible to use a melting process (direct fusion) in presence of modest pressure with heat transfer or it can use adhesive materials that joins the parts through superficial chemical reactions. The first two techniques create strong covalent type bonds, but they have the disadvantage to demand extremely smooth and clean surfaces for being effective, as the first step for a good resolution of the fusion is to bond the surfaces by the Van der Waals intermolecular forces. The product quality is correlated to the process temperature, between the 800°C and the 1200°C, levels of equal resistance than the crystalline structure of the same material are achieved, but already between 200°C and the 400°C sufficiently strong bonds are realized by the chemical activation of surface reactions. To improve the fusion a solution obtained from the combination of the several procedures can be used. The alignment of the layers, thanks to laser techniques, reaches precisions of the order of the μm, even if, currently, it is not possible to align more than 5-6 wafer maintaining such accuracy.

6.3 Micro Reaction Sintering (MRS)

This manufacturing techniques is developed for the production of SiC turbomachines rotors of 5÷10 millimetre of diameter. From graphite powders, α-SiC, silicon phenol resin is inserted in a stamp, derived from silicon wafer. The parts of the stamp are melted and all component is submitted to high temperature HIP. The technique has been calibrated in several conditions of pressure, temperature and composition of base powders and it has been verified that the microcrystalline structure of the final piece has an higher quality if the furnace temperatures is about 1500-1700°C, the pressure varies from 100 to 50 MPa and using α-SiC powders instead of silicon one. A microscopic analysis of the structure has demonstrated that melted stamp reacting with the graphite substrate forms a covering of β-SiC around a nucleus of α-SiC deriving from initial powders. But is not still available

mechanical tests on the material. The adoption of this technique wants substantially to reduce the excessive long times of bonds production of the CVD or the DRIE on SiC wafer, caused by the speed of material deposition and recording, and to the lack of accuracy of the EDM (Electro Discharge Machining).

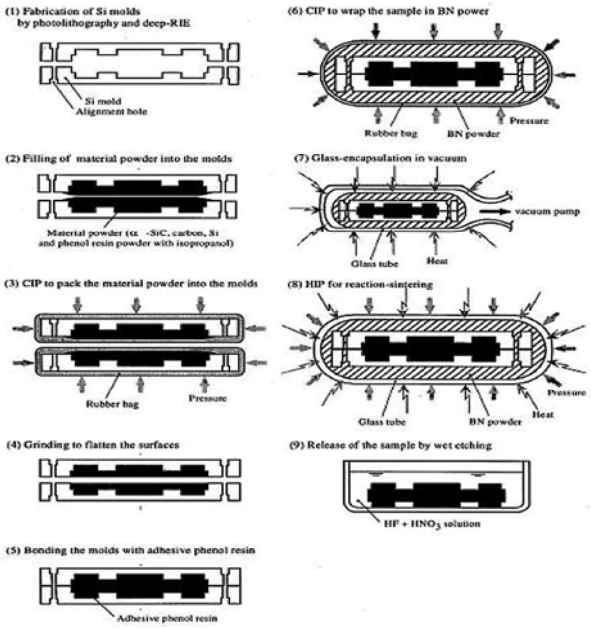

Fig. 28. Micro Reaction Sintering phases

7. Economic overview analysis and potentialities

All possible application and the alternatives of the proposed device must be investigated. It appears obvious that a UMGT will be utilized in the two main area, already covered by the large scale machines:

- the power generation
- the vehicle propulsion.

The primary application filed will be the first one; the higher energy density respect to a chemical battery with an overall efficiency of the 5-10% is sufficient to render a UMGT more attractive on the market. Substantially fuel tank is the bigger component, for which reason, in the developments of such machine, the researchers have to obtain low consumption than to high power output, thanks to the possibility to satisfy the power requirements through "modular clusters". Besides the possibility to feed every type of portable device, a such generator could go satisfy the power requirements of aircraft onboard systems, in terms of redundancy and higher operational temperatures, in comparison to the conventional battery packages. The competition with the large scale power plant is not possible, because is not imaginable of achieve efficiency of the order of 50-60%. The situation would be various in the moment in which will be possible to obtain, for example with regeneration, efficiencies

about 20-30%. So the lower performances could be compensated with the advantage of the redundancy, the lowest noisiness and the UMGTs compactness. Such levels are still the much far being reached. On the other hand, in the emergency applications, where the efficiency is not a limiting requirement regarding the compactness, succeeding to contain the costs, a UMGT would not have rivals. Three requirement that render this device a lot attractive are therefore, compactness, redundancy and lower noisiness thanks to the speed frequencies of hundred of kHz (beyond the audibility threshold) and to the length small scale (the exit flow is quickly stirred with the surrounding atmosphere). In propulsion system this device is considered as one of the more attractive relatively to little reconnaissance planes (100-1000 g of takeoff weight), thanks to the high thrust/weight ratio, which scale with the inverse of the length. The ICE motors currently under construction for these applications, are ten times greater, much noisy and with greater fuel consumptions. The possibility to use UMGT cluster, for the propulsion of great aircrafts is remote, as it seems improbable to succeed to obtain lower consumption to performance parity, without to count eventual difficulties of assembling process, due to the elevated number of necessary devices (at least 10^5). The determining factor in the diffusion of a UMGT system resides , however, in the production cost. In fact, the production of this devices presents high manufacturing cost, tied to the complex technologies to adopt, amortizable with the production in large series scale. According to an esteem of the MIT (a CMOS silicon wafer of 200 of millimetre of diameter can cost $ 600-1000), if produced in large scale, a wafer of MEMS generators could produce several kW to the cost of several thousands of dollars for the fabrication. The result is a specific cost of 0,5-5 $/W. Other considerations have to be done for civil application and for higher power rate (within the UMGT power rate). Here below it is discussed a practical case study.

8. User definition

8.1 UMGT advantages

The main advantage of these systems compared to the existing large scale devices resides in the highest power density. Although such systems have an overall efficiency still lower, the produced power for weight unit is the higher than which will be produced by the battery systems. In fact, at the moment, the battery package power density is about 100-150 Wh/kg. Even if an increase of the power density can be presupposed, the power developed by a UMGT is, undoubtedly, higher for weight and volume unit. Also with a lower efficiency the UMGTs have a power density that is, at least, equivalent to that theoretically produced by a lithium battery package It will be noticed, then, as in the field of the same micro turbines, there is a difference, in terms of performances, according to the used fuel: for instance, the combustion of the hydrogen, in fact, concurs to remarkably raise the value of the power density regarding the obtainable result with fuel like propane or kerosene. An ulterior advantage is the operating flexibility that offers such systems: while the battery package, once exhausted theirs energetic potential, need of a period, more or less long, to recharge them, the micro turbines allow the fuel change in a very short period.

8.2 UMGT disadvantages

The main disadvantage, respect fuel cells or the battery package, is the high operational temperature. In fact, to achieve an higher output power is necessary to realize high TIT. Because of the small scale of the machine, this design constraint leads all the system to raise

own average temperature: this produces high infrared radiation emissions, that, especially in military applications, cannot be tolerated. A similar problem is found in the fuel cells in which, a lower value of the operational average temperature is reached. That infrared emissions is not the only problem for the UMGT. The high outlet temperatures of the exhaust gas, can produce problems during the operational life of the machine. To obviate to such disadvantage a regenerator, even built-in would have to be installed inside the device, to cooling the UMGT components using Peltier effect.

8.3 UMGT potential application

Multiple applications can be easy found for UMGT systems. In general terms, these ones can be divided in two groups: applications as portable power generation systems or as range extender/prime mover in different vehicles (wheel vehicles, aircraft, ecc).

8.3.1 Portable power generation

Regarding this use it can be distinguished military uses and civil applications, even if, these last one, have very limited use possibility.

8.3.1.1 Military applications

The power demand of a soldier during a mission is remarkably increased during the last few years due to the adoption of new technologies. At the same time we have the necessity to limit the most possible equipment weight for the unit. In this case, use an UMGT could help in the reduction of the transported load and, at the same time, satisfy the power demand. Some of these applications are shown in figure 29.

Fig. 29. The "future" soldier

We can distinguish three various regimes for the military applications:

$$\text{medium power} \begin{cases} 20\text{W, with peaks of } 50\text{W}, \\ 100\text{W, with peaks of } 200\text{W} \\ 1000\text{W, with peaks of } 5000\text{W} \end{cases}$$

The first group of device generates the required power for computer, radius and sensors. The second one finds application in the laser beam and the conditioning of the soldiers (uniform ventilation in external extreme climatic conditions); with this powers range the

loading of batteries is possible too. At last, 1-5 kW could be used for feeding of exoskeleton : these are robotic devices that allow to reduce the payload that weighs on the soldier.

8.3.1.2 Civil applications

The UMGT civil applications, as portable power generators, undoubtedly are limited, due to the high system temperature. In fact, in this case the exhaust gas temperature is very high, and the customer safety is a primary objective in the design of the device and its utilization. However, some civil applications can be considered, as battery recharger for mobiles or for wireless tools. Also as micro cogeneration unit at small scale.

8.3.2 MAV

The main application in this field resides in the so-called the MAV (micro aerial vehicles). Their main use is, once again, of military character. The power demanded by the group is lower because the considered vehicle mass is lower than 50 g with cruise speed between the 10 and 20 m/s: in the cruise regime the shaft demanded power is about 2.5 kW, while this doubles during the phase of takeoff and manoeuvres. Due to the high heat exchange during the flight and the low required power, there are not problems regarding the infrared emissions. Such systems have already been used in the Balkans, Afghanistan and Iraq during missions of strategic character.

8.3.3 Drones and UAV

An unmanned aerial vehicle (UAV) is a machine which functions either by the remote control of a navigator or pilot or autonomously, that is, as a self-directing entity. Their largest use is within military applications. To distinguish UAVs from missiles, a UAV is defined as a powered, aerial vehicle that does not carry a human operator, uses aerodynamic forces to provide vehicle lift, can fly autonomously or be piloted remotely, can be expendable or recoverable, and can carry a lethal or non lethal payload". UAVs typically divided in six functional categories (although multi-role airframe platforms are becoming more prevalent):

- Target and decoy – providing ground and aerial gunnery a target that simulates an enemy aircraft or missile
- Reconnaissance – providing battlefield intelligence
- Combat – providing attack capability for high-risk missions (see Unmanned combat air vehicle)
- Logistics – UAVs specifically designed for cargo and logistics operation
- Research and development – used to further develop UAV technologies to be integrated into field deployed UAV aircraft
- Civil and Commercial UAVs – UAVs specifically designed for civil and commercial applications

They can also be categorized in terms of range/altitude and the following has been advanced as relevant at such industry events as Unmanned Systems forum:

- Handheld 600 m altitude, about 2 km range
- Close 1,500 m altitude, up to 10 km range
- NATO type 3,000 m altitude, up to 50 km range

- Tactical 5,500 m altitude, about 160 km range
- MALE (medium altitude, long endurance) up to 9,000 m and range over 200 km
- HALE (high altitude, long endurance) over 9,100 m and indefinite range
- HYPERSONIC high-speed, supersonic (Mach 1–5) or hypersonic (Mach 5+) 15,200 m or suborbital altitude, range over 200 km
- ORBITAL low earth orbit (Mach 25+)
- CIS Lunar Earth-Moon transfer
- CACGS Computer Assisted Carrier Guidance System for UAVs

8.3.4 Range extender in hybrid vehicle

In the last decade, governmental incentives and the ever stricter emissions regulations have prompted some of the largest world automakers to dedicate resources to the study, design, development and production of hybrid vehicles, which offer undisputed advantages in terms of emissions and fuel consumption with respect to traditional, reciprocating internal combustion engines. In fact, hybrid engines are substantially smaller than conventional ICE, because they are designed to cover the vehicle's "average" power demand, which ensures proper traction for about 99% of the actual driving time, and is exceeded only for prolonged mountain drives and instantaneous accelerations. When excess power is needed above this average, the hybrid vehicle relies on the energy stored in its battery pack. Hybrid cars are often equipped with braking energy recovery systems that collect the kinetic energy lost in braking, which would be dissipated into heat otherwise, and use it to recharge the battery. Smaller sizes and an (almost) constant operational curve lead to lower emissions. Moreover, a hybrid vehicle can shut down completely its gasoline engine and run off its electric motor and battery only, at least for a limited operational range: this "mixed operation" increases the net mileage and releases a substantially lower amount of pollutants over the vehicle lifetime. The most popular hybrid vehicles (HV) are mostly passenger hybrid cars equipped with a traditional ICE and an electric motor coupled in parallel. The thermal engine is sized, with some exceptions, for the average power, and the surplus power needed during rapid acceleration phases is supplied by the electric motor.

9. Distance between state of art and goals

From the analysis of the several prototypes and from the documentation available in literature and on the web it can be noticed as all the groups of search are to the state of prototype. Regarding the prototype of the MIT they have been found problems of rotors failure in operating conditions. The group design by the Belgian researchers seem to be at the more advanced state, but they are not available data of any application. The Japanese model has been introduced to meeting a NATO and lacks recent news. For the Italian model the problem, currently resides in leading the system to a rotational speed, by means of generator/ electric motor, sufficient to prime the combustion. Problems have been found in the bearings behaviour and their limited lifetime

10. Conclusions

Here follow the several problems that affect this technology have been listed, as eventually exceeding these design, manufacturing and realization problems, for a device mass production.

a. The thermodynamic cycle

It is a "standard" Brayton cycle, usually adopted in large scale turbogas. With the exception of the industrial cycles, for constructive reasons, the compression ratio is extremely low in this UMGT ($p_2/p_1 \approx 2$), and therefore the total efficiency of the machine is corresponding low (7-8%). Increase of the compression ratio, recovery of the heat of the gas are possible modifications under investigation, to increase such efficiency: but such upgrading appear difficult to implement on an UMGT device.

b. The fuel choice

The fuel used, suggested, chosen for all prototype is a liquid hydrocarbon (pentane-butane or similar). The kerosene use or other jet-fuel appears perfectly compatible. For the operational prototype, the possibility is being studied to use methane or hydrogen, but this last one generates problems of tank design (high pressure, low power density).

c. Design problems

The analysis of existing prototypes indicates as the main design problems that can be previewed to this point are the following ones:

1. combustion chamber: low residence times (flammability threshold); mixing device; resistance to the high temperatures;
2. bearings: reliability, duration (to the highest rotational speed);
3. rotors: radial and bending/torsion instability, resistance to the high temperatures;
4. electric generators: practical feasibility and reliability, efficiency problems;
5. controls devices: stability, reliability;
6. thermo-fluid dynamic analysis: reliability of the design procedures, based on experiences achieved exclusively on large scale devices. The first simulations have evidenced the necessity to adopt scale factors in the turbomachines design.

d. Technological and manufacturing problems

They are generally correlated to the availability of opportune high resistance materials (high thermo mechanical stresses) as well as the combustion chamber, turbine, regenerator, ecc. And to the productive technologies. While such problems will not have great influence on the realization of the prototypes, an engineering study to pass "to the productive" part (post-prototypal phase) will be necessary. Finally, the economic impact of these devices will be dependent on the performance levels and the manufacturing costs, both of which have yet to be proven. It is certainly possible, however, that UMGTs may, one day, be competitive with conventional machines in a cost per installed kilowatt. Even at much higher costs, they will be very useful as compact power sources for portable electronics, equipment, and small vehicles.

11. References

[1] A.H. Epstein, S.A. Jacobson, J.M. Protz, L.G. Frechette, "*Shirtbutton-sized gas turbines: the engineering challenges of micro high speed rotative machinery*"; Proc. 8th Int. Symposium. on Transport Phenomena and Dynamics of Rotating Machinery (ISROMAC-8), Honolulu HI, March 2000.

[2] A.H. Epstein, *"Millimetre-scale, MEMS gas turbine engines"*; Proc. ASME Turbo Expo 2003; June 2003, Atlanta USA.
[3] J. Shepherd, "*Principles of Turbomachinery*", J. Macmillan Pub. Co, NY 1956.
[4] V. Zucrow, Hoffman "*Gas dynamics I, Vol.1*".
[5] R. Capata, E. Sciubba *"A study on thermodynamic feasibility and possible utilization of nano gas turbines"*, ICAT 2005, Istanbul, May 2005.
[6] R. Capata, E. Sciubba: IMECE2007-42118: "*Design and Performance Prediction of a Ultra-Micro Gas Turbine for Portable Power Generation*" Proceedings of IMECE2007, November 12-17, Seattle, Washington, 2007.
[7] R. Capata, E. Sciubba: IMECE2009-12281: "*The α-prototype of an ultra-micro-gas turbine at the University of Roma 1. Final assembly and tests*". Proceedings of IMECE2009, November 11-16, Orlando , Florida, 2009
[8] C.M., Spadaccini Mehra A., Lee J., Lukachko S., Zhang X., Waitz I.A. "*High Power Density Silicon Combustion System for Micro Gas Turbine Engines*", Paper GT-2002-30082, ASME International Gas Turbine Institute TURBO EXPO '02, Amsterdam, The Netherlands.
[9] S. Kang, J. P. Johnston, T. Arima, M. Matsunaga, H. Tsuru, F. B. Prinz, "*Micro-scale radial-flow compressor impeller made of silicon nitride-manufacturing and performance*", Proc. ASME Turbo Expo June 2003, GT2003-38933.
[10] Balje, O., "*Turbomachines*", J. Wiley & Sons, 1981.
[11] Moon, H. S., Choi, D., Spearing, S. M. "*Development of Si-SiC Hybrid Structures for Elevated Temperature Micro-Turbomachinery*", J. Micro-electromechanical systems, vol. 13, no. 4, Aug 2004.
[12] Munro, R. G., "*Material Properties of a Sintered a-SiC*", J. Physical and Chemical Reference Data, Vol. 26, pp. 1195-1203 (1997), American Chemical Society.
[13] Peirs, J., Reynaerts, D., Verplaetsen, F., Norman, F., Lefever, S. "*Development of a Micro Gas Turbine for Electric Power Generation*", BE Paper Eurosensors 2003.
[14] Sciubba E., "Turbomachinery: notes", 2001Euroma, Italy.
[15] Sugimoto, S., Tanaka, S., Li, J. F., Watanabe, R., Esashi, M. "*Silicon Carbide Micro-reaction-sintering Using"*.
[16] www.alcatel.com, "*'I-Speeder' the future DRIE etching tool for MEMS*", April 2000, Bosch, Alcatel, PerkinElmer.
[17] Frechette L. G., Jacobson S. A., Breuer S. K., Ehrich F. F., Ghodssi R., Khanna R., Wong C. W., Zhang X, Schimdt M. A., Epstein A. H. "*Demonstration of a micro-fabricated high-speed turbine supported on gas bearings*", BE Paper Eurosensors 2003.
[18] Jacobson S. A., Epstein A. H., "*An informal survey of power MEMS*", 2003, Inter. Symp. On Micro-Mech. Engin., Dec. 2003.
[19] ATIP Scoop, Japan Office, "*Micro Gas Turbine Development*", Feb 2005.
[20] Esashi M., "*Microsystems by bulk micromachining*" .
[21] www.mems-exchange.org/catalog/P3271/
[22] Abbott I. H., "*Theory of wing sections*" 1959, Dover Publ. Inc., New York.
[23] Song B., "*Experimental and Numerical Investigation of optimized high-turning Supercritical Compressor Blades*", PhD dissertation in Mechanical Engineering at Virginia Polytechnic Institute 2002.
[24] Butler R. J., Byerley A. R., VanTreuren K., Baughn J. W., "*The effect of turbulence intensity and length scale on low-pressure turbine blade aerodynamics*", Int. J. Heat and Fl. Flow 22 (2000) pp. 123-133.

[25] Choi J., Teng S., Han J., Ladeinde F., "*Effect of free-stream turbulence on turbine blade heat transfer and pressure coefficients in low Reynolds number flows*", Int.. J. Heat Mass Transfer 47 (2004) pp. 3441-3452.

[26] Park T. S., Sung H. J., "*A nonlinear low-Reynolds number k-epsilon model for turbulent separated and reattaching flow*", Int. J. Heat Mass Transfer Vol.38, No 14, pp 2657-2666 , 2003.

[27] Gaydamaka I. V., Efimov A. V., Ivanov M. Ja., Ivanov O. I., Nigmatullin R. Z., Ogarko N. I., "*Some Aerodynamic Performances of Small Size Compressor and Turbine Stages*", Proc. Int. Gas Turbine Congress 2003 Tokyo.

[28] Waits C. M., Modale A., Ghodssi R., "*Investigation of gray-scale technology for large area 3D silicon MEMS structures*", J. Micromechanics and Micro-engineering, 13 (2003) pp. 170-177.

[29] Lin C. C., Ghodssi R., Ayon A. A., Chen D. Z., Jacobson S., Breuer K., Epstein A. H., Schimdt M. A., "*Fabrication and Characterization of a Micro Turbine/Bearing Rig*", 1999.

[30] R.A. Van Den Braembussche, A.A.Islek, Z. Alsalihi: "*Aerothermal Optimization Of Microgasturbine Compressor Including Heat Transfer*", Proc.Int. Gas Turbine Congress 2003, Tokio.

[31] Ishihama, Y. Sakai, K. Matsuzuki, T. Hikone"*Structural Analysis Of Rotating Parts Of An Ultra Micro Gas Turbine*" Proc. Int. Gas Turbine Congress 2003 Tokio, November 2-7, 2003.

[32] I.V. Gaydamaka, A.V. Efimov, M. Ja. Ivanov, O.I. Ivanov, R.Z. Nigmatullin, N.I. Ogarko Turbine Department: "*Some Aerodynamics Performances Of Small Size Compressor And Turbine Stages*" Proc. Int. Gas Turbine Congress 2003 Tokio November 2-7, 2003.

[33] J.P. Johnson, S. Kang, M. Matsunaga, H. Tsuru, F.B. Prinz,: "*Performance Of Micro-Scale Radial Flow Compressor Impeller Made Of Silicon Nitride*". Proc. Int. Gas Turbine Congress 2003 Tokio, November 2-7, 2003.

[34] K. Matsuura, C. Kato,H. Yoshiki, E. Matsuo, H. Ikeda, K. Nishimura, R. Sapkota: "*Prototyping Of Small-Sized Two Dimensional Radial Turbines*" Proc. Int. Gas Turbine Congress 2003 Tokio, November 2-7, 2003.

[35] T. W. Simon, N. Jiang: "*Micro -Or Small-Gas Turbines*" Proc. Int. Gas Turbine Congress 2003 Tokio, November 2-7, 2003.

[36] Iwai: "*Thermodynamic Table For Performance Calculations In Gas Turbine Engine*" Proc. Inte. Gas Turbine Congress 2003 Tokio, November 2-7, 2003.

[37] M.A. Schmidt: "*Technologies For Microturbomachinery*"

[38] L.G. Frechette; S.A. Jacobson, K.S. Breuer, F.F. Ehrich, R. Ghodssi, R. Khanna, C.W. Wong, X. Zhang, M.A. Schmidt, A.H. Epstein, "*Demonstration Of A Microfabricated High-Speed Turbine Supported On Gas Bearings*" , Proc. Int. Gas Turbine Congress 2003 Tokio, November 2-7.

[39] A.H. Epstein, S.D. Senturia, O. Al-Midani, G. Anathasuresh, A. Ayon, K. Breuer K-S Chen, F.F. Ehrich, E. Esteve, L. Frechette, G. Gauba, R. Ghodssi, C. Groshenry, S.A. Jacobson, J.L Kerrebrok, J.H. Lang, C-C Lin, A. London, J. Lopata, A. Mehra, J.O. Mur Miranda, S. Nagle, D.J. Orr, E. Piekos, M.A. Schmidt, G Shirley, S.M. Spearing, C.S. Tan, Y-S Tzeng,I.A. Wait: "*Micro-Heat Engines, Gas Turbines, And Rocket Engines -The Mit Microengine Project*" 28th AIAA Fluid Dynamics Conference, 4th AIAA Shear Flow Control Conference, June29-July 2,1997, Snowmass village CO.

[40] Epstein,: *"Millimetre scale, MEMS Gas Turbine Engine"* Proceedings of ASME Turbo Expo 2003 Power for Land, Sea, and Air, June 16-19, 2003, Atlanta, Georgia, USA GT-2003-38866

[41] Liu, T.F. Enrich, L. Ho, H Li, S. Jacobson, Z.S. Spakovszky: "*High Speed Micro-Scale Gas Bearings For Power MEMS*", MTL Annual Report 2005.

[42] Epstein, S.A. Jacobson, J.M. Protz, C. Livermore, J. Lang, M. Schmidt: "*Shirtbutton-Sized, Micromachined, Gas Turbine Generators* 39th Power Sources Conference, Cherry Hill, NJ,June 2000.

[43] L-A Liew, W. Zang, L. An, S. Shah, R. Luo, Y. Liu, T. Cross, M. L. Dunn , V. Bright, J.W. Daily, R. Raj: "*Ceramic MEMS- new Materials, Innovative Processing and Future Applications"* American Ceramic Society Bulletin, Vol 80, No.5.

[44] S. Martinez Romero, "*Multipoint Optimisation Of A 2d Compressor With Splitters For A Micro-Gas Turbine Application*" 2003.

[45] A.H. Epstein, S.D. Senturia, G. Anathasuresh, A. Ayon, K. Breuer K-S Chen, F.F. Ehrich, G. Gauba, R. Ghodssi, C. Groshenry, S.A. Jacobson, J.H. Lang, C-C Lin, A. Mehra, J.O. Mur Miranda, S. Nagle, D.J. Orr, E. Piekos, M.A. Schmidt, G Shirley, S.M. Spearing, C.S. Tan, Y-S Tzeng, I.A. Waitz: "*Power MEMS And Microengines* IEEE Transducers '97 Conference, Chicago, IL, June 1997.

[46] R.A. Van den Braembussche, web paper: *"Thermo-Fluid-Dynamic Design Of Ultra Micro Gas-Turbine Components"*.

[47] Web: *MEMS GUIDE* (http://www.memsnet.org/mems/processes/).

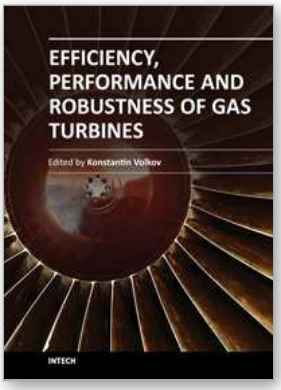

Efficiency, Performance and Robustness of Gas Turbines
Edited by Dr. Volkov Konstantin

ISBN 978-953-51-0464-3
Hard cover, 238 pages
Publisher InTech
Published online 04, April, 2012
Published in print edition April, 2012

A wide range of issues related to analysis of gas turbines and their engineering applications are considered in the book. Analytical and experimental methods are employed to identify failures and quantify operating conditions and efficiency of gas turbines. Gas turbine engine defect diagnostic and condition monitoring systems, operating conditions of open gas turbines, reduction of jet mixing noise, recovery of exhaust heat from gas turbines, appropriate materials and coatings, ultra micro gas turbines and applications of gas turbines are discussed. The open exchange of scientific results and ideas will hopefully lead to improved reliability of gas turbines.

InTech Europe
University Campus STeP Ri
Slavka Krautzeka 83/A
51000 Rijeka, Croatia
Phone: +385 (51) 770 447
Fax: +385 (51) 686 166
www.intechopen.com

InTech China
Unit 405, Office Block, Hotel Equatorial Shanghai
No.65, Yan An Road (West), Shanghai, 200040, China
中国上海市延安西路65号上海国际贵都大饭店办公楼405单元
Phone: +86-21-62489820
Fax: +86-21-62489821